بسم الله الرحمن الرحيم

Palestine Polytechnic University

College of Engineering & Technology
Mechanical Engineering Department

Graduation Project

Cargo Planar Vibration Control of a Ship-mounted crane

Project Team
Jebreen Fakhouri
Mohammad Al-Rjoub
Sulieman Al-Sweity

Project Supervisor
Dr. Yousef M. Al-Sweiti

Hebron-Palestine

May, 2007

Abstract

This work deals with mathematical modeling, simulation and control of a ship-mounted cranes which have the Maryland Rigging. The developed model contains three independent inputs to control the vibrations in the plane of the boom; the luff angle is utilized to ensure the controllability of the rigid boom, and the total length of the upper cable in conjunction with the position of its lower suspension point are used to guarantee the controllability of the payload. The disturbances acting on the ship due to sea motions is represented by the rolling displacement of the ship about its center of gravity, the heave motion from the sea in the vertical direction, also the excitation in the horizontal direction that comes from the sea motion in that direction, and an external force acting directly to the payload usually caused by winds. The full nonlinear model of the crane is developed and then converted to linear model using Taylor series to expand nonlinear terms about the current equilibrium point. After the linearization process we deal with the state space representation for simulation purposes. This system will be controlled using state feedback optimal method, and the unknown disturbances were estimated using PI extended observer, then simulation results for one operating point and all admissible operating points were performed.

Table of Contents

Chapter Three
Linearization and State space representation

Chapter Four
Control system design

Chapter Five

List of Figures

Notations

L_1, L_2	segments length of the upper cable
L, l	length of the upper cable and length of the payload cable
L_3, L_4, L_5	Geometrical parameters of the crane
D, ρ	position of the lower suspension point and luff angle
$\alpha_1, \alpha_2, \varphi_2$	angle of L_1 with the horizontal, angle of L_2 with the horizontal, and angle of l with the vertical
β, δ	angle of the boom with the horizontal and roll angle
x_i, y_i	x and y coordinates of m_i, i =1,2
$p_2, \hat{p}_2$	actual and estimated disturbance force
$x_G, \hat{x}_G$	actual and estimated sea waves disturbance through x-excitation
m_1, m_2	mass of the pulley, payload, and member BC
M	sum of the two masses
M_0, K_0	mass and stiffness matrices
B_1, B_3	input matrices
B_2, B_4, B_5, B_6, B_7	disturbances matrices
B, B_e	input and extended input matrices
u, y, y_m	input, output, and measurement vectors
$q, z, \hat{z}$	displacement vector, state vector, and estimated state vector
A, A_e	system and extended system matrices
B, B_e	input and extended input matrices
E, E_e	disturbance and extended disturbance matrices corresponding to rolling
N	disturbance matrix corresponding to the wind force acting on the payload
C, C_e	output and extended output matrices
F	disturbance matrix corresponding to the disturbance x_G
D	input feed forward matrix
E_0, F_0	disturbance feed forward matrices, corresponding to the rolling and x_G disturbances
L_1, L_2, L_3, L_e	observer gain components and extended observer gain matrix
λ_i	i^{th} eigenvalue

e, J	error vector and input matrix for the error equation of the observer
Q, Q_e	weight matrix of the states and the estimated states for the optimal design
R, R_e	weight matrix of the inputs and the measurements for the optimal design
P	solution of Ricatti equation
u_ϕ, K_ϕ	input vector and gain of the rolling disturbance compensator
u_z, K_z	input vector and gain of the optimal controller
u_{x_0}, K_{x_0}	input vector and gain of the sea waves disturbance compensator

Chapter one

Introduction

1.1 Overview

Ship-mounted cranes are a ships of multiple sizes with cranes mounted on the ship board, and they are used to transfer cargo from one ship to another in an open sea as shown in Fig. (1.1). They are used also at port to transfer cargo from large ships to lighter port-going vessels when ports of deep water are not available. During the transfer process, wave-induced motions of the crane can produce large oscillations of the cargo being hoisted, especially if the exciting frequency coming from the sea waves is close to the resonance frequency of the crane. This endangers the operation of the crane and forces the cargo transfer to be suspended.

Figure (1.1) : Picture of a ship-mounted crane at sea

1.2 Literature review

Ship-mounted cranes are discussed in the last few years in several publications. Yuan et al. [24] proposed the "Maryland's Rigging" and applied a brake system to the upper cable as it passes over the pulley, Kimiaghalam et al. [9] proposed a fuzzy controller to limit the pendulation of the payload by changing the length of the upper cable, Dadone and Van Landingham [4] proposed fuzzy logic for controlling the Coulomb friction in the pulley, Kimiaghalam et al. [10] proposed feedback and feed forward control law to change the luff angle and the length of the rope. Mr. Al-swieti [1] studied the control of elastic ship-mounted crane Using Variable-Gain Model-Based Controller in his PHD

1.3 Modified crane configuration

In this work the team studied the vibration control problem of the modified crane configuration with "Maryland's Rigging" as shown in the Fig. (1.2). The crane is provided with three inputs to control the planer vibration of the payload:

1. The length of the upper cable $L(t)$, where $L(t)=L_1(t)+L_2(t)$.
2. The boom luff angle ρ.
3. The distance $D(t)$, of the lower suspension point B' along the boom.

Also in this study four disturbances will be considered to be acting on the system, and these disturbances are:

1. p_2: Wind force or any disturbing force acting directly on the payload.
2. $\Delta\delta$: Ship rolling due to the sea motion.
3. y_0: Heave motion of the ship (displacement in the y direction).
4. x_0: Displacement of the ship in the x direction.

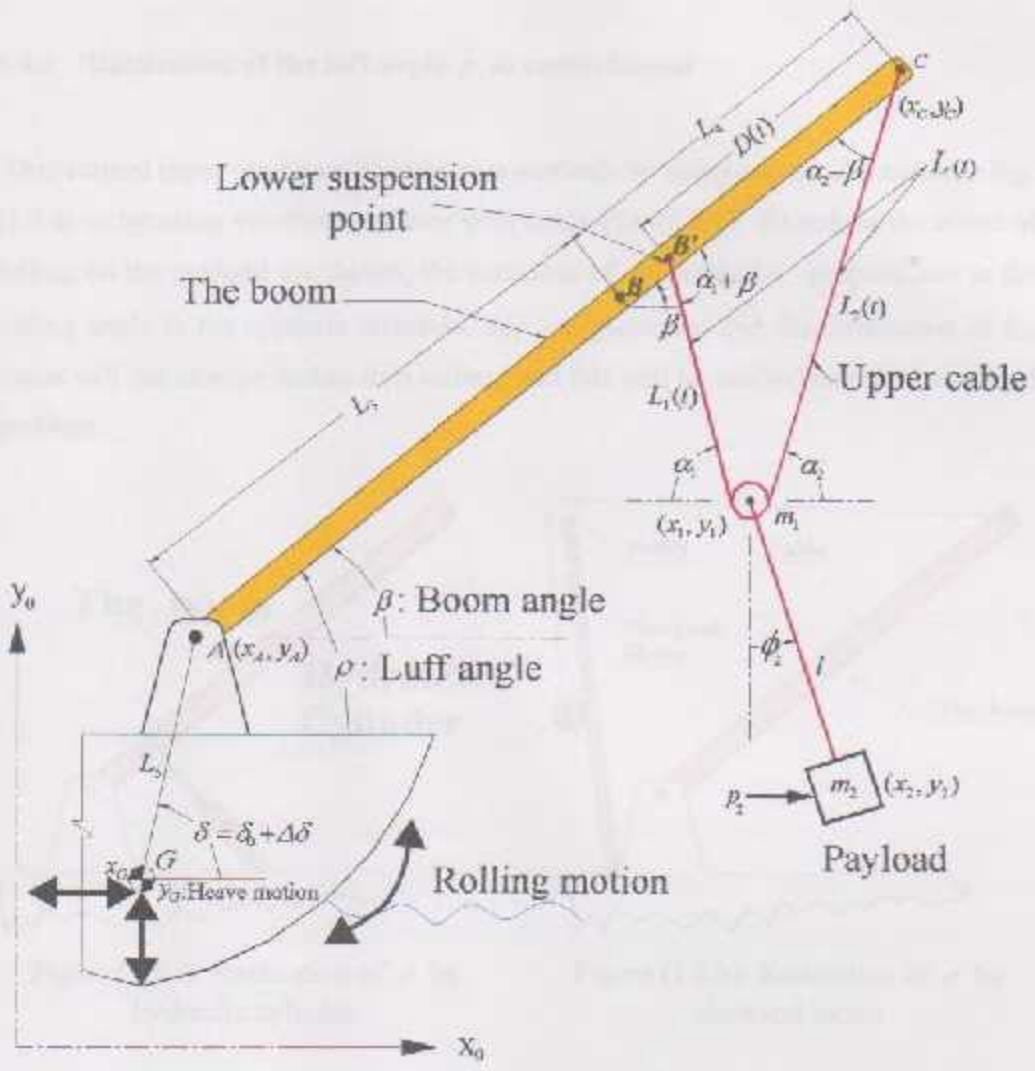

Figure (1.2): modified crane configuration

1.4 Realization of the control inputs

For any system to be useful it must be realizable, and beside this some terms will be misleading till the way of realizing the supposed control inputs is explained, and this is the aim of this section.

1.4.1 Realization of the luff angle ρ as control input

This control input can be realized by two methods by using a hydraulic cylinder Fig. (1.3.a) or by using electrical actuator with cable Fig. (1.3.b). To reduce the effect of rolling on the payload oscillation, the actuation of ρ should be proportional to the rolling angle in the opposite direction, this can guarantee that the orientation of the boom will not change during ship rolling, and this will be studied later in the control problem.

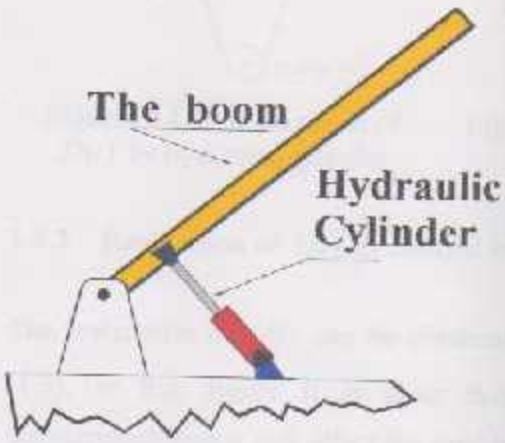

Figure (1.3.a): Realization of ρ by hydraulic cylinder

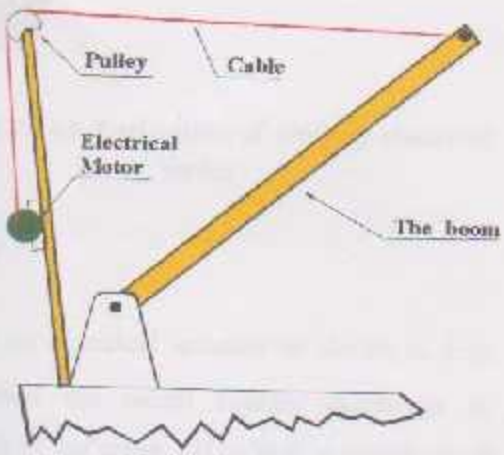

Figure (1.3.b): Realization of ρ by electrical motor

1.4.2 Realization of $D(t)$ as control input

This control input can be realize by two methods, one is by using a hydraulic cylinder Fig. (1.4.a), and the other one is by using electrical actuator, the principle of using the electrical actuator is shown in Fig. (1.4.b) where B' will move to the right or to the left according to the rotation direction of the motor. It should be mentioned

here that the motion of B' along portion BC will not effect the total length of the cable $L(t)$, it is mainly used to effect on the x position of the payload.

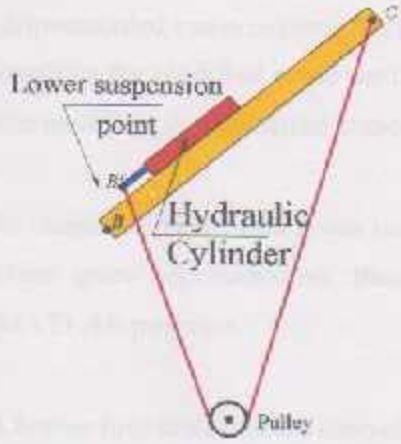

Figure (1.4.a): Realization of $D(t)$ by hydraulic cylinder

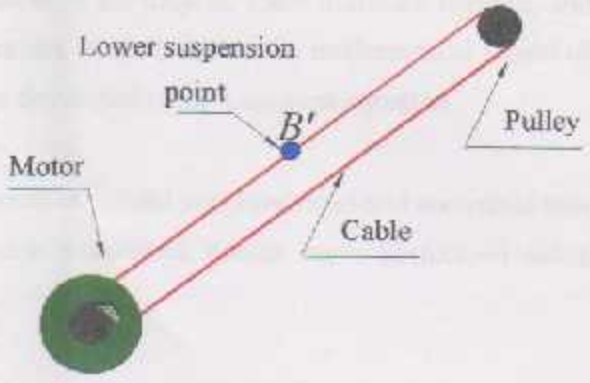

Figure (1.4.b): Realization of $D(t)$ by electrical motor

1.4.3 Realization of $L(t)$ as control input

The realization of $L(t)$ can be obtained by an electrical actuator as shown in Fig. (1.5), in this figure it is clear that when the motor rotates clockwise or counterclockwise it will effect the total length of the cable $L(t)$ which is mainly used to effect on the y position of the payload.

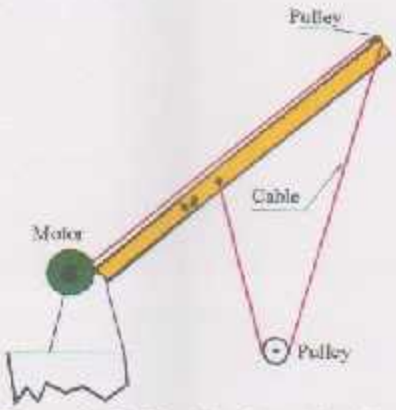

Figure (1.5): Realization of $L(t)$

1.5 Project scope

This thesis will contains five chapters chapter one gives a brief introduction to the ship-mounted crane system, the problem of the project, some literature reviews, and explains the modified crane configuration. In chapter two the mathematical model of the modified ship-mounted crane was developed using Lagrange equation.

In chapter three the non linear mathematical model was linearized and converted into state space representation, then some simulation results were performed using MATLAB program.

Chapter four concerns the controller design to suppress vibrations of the payload, and the observer design which will estimate the unmeasured states and disturbances.

Finally in chapter five, the results and conclusions were established in addition to some recommendations for future studies.

Chapter two
Model development

This chapter deals with the model development of the ship-mounted cranes, which have the modified Maryland rigging design. The dynamics of the system is expressed by using Lagrange's formulation; three inputs are used to control the planar vibrations of the payload due to three types of base excitation. The model is limited to the in-plane oscillations because those have the most dangerous effect in practical applications.

The disturbances acting on the system are represented by the rolling displacement of the ship $\Delta\delta$ due to sea waves, the wind force p_2 acting directly on the payload, the excitation in the y-direction y_G (heave motion), and the horizontal excitation in the x-direction x_G see Fig. (1.2).

2.1 Assumptions

In deriving the mathematical model of the crane, the following assumptions are considered:

- The boom is rigid.
- The mass of the cables is neglected.
- The elastic elongations of the cables are neglected.
- The lower suspension point B' of the upper cable is movable along the rigid boom.
- The pulley m_1 riding on the upper cable is frictionless.
- Dynamics of all actuators will not be considered.

• The angle β represents the orientation of the boom axis with respect to the Horizontal. It is equal to the (algebraic) sum of the roll angle $\Delta\delta$ and the luff angle ρ.

• The disturbances acting on the crane are the rolling, heave and the displacement in the horizontal direction of the slup due to sea motions in addition to the force p_2 acting directly on the payload; this force may appear due to a strong wind or a direct impact force which may happen by accident during the operation of the crane.

2.2 Kinematics of the upper cable

With reference to Fig. (1.2), it is assumed that L_1 and L_2 are the distances between the pulley and the lower and upper suspension points (B' and C) respectively. By applying the sine law, these distances can be expressed as

$$L_1 = D\sin(\alpha_2 - \beta)\csc(\alpha_1 + \alpha_2) \tag{2.1}$$

$$L_2 = D\sin(\alpha_2 + \beta)\csc(\alpha_1 + \alpha_2). \tag{2.2}$$

then the total length of the cable is given by

$$\begin{aligned} L(t) &= L_1 + L_2 \\ &= D\cos\left(\beta + \frac{\alpha_1 - \alpha_2}{2}\right)\sec\left(\frac{\alpha_1 + \alpha_2}{2}\right) \end{aligned} \tag{2.3}$$

where α_1 and α_2 denote the angles of L_1 and L_2 with respect to the horizontal, D represents the position of the movable suspension point B' along the boom with respect to the tip of the boom, and

$$\beta = \rho + \Delta\delta \tag{2.4}$$

where ρ denotes the luff angle of the boom, and $\Delta\delta$ denotes the ship rolling angle due to sea motions. Applying the cosine law to the triangle spanned by L_1, L_2, and D gives

$$L_1^2 = L_2^2 + D^2 - 2L_2 D\cos(\alpha_2 - \beta) \tag{2.5}$$

the length L_1 can be expressed as

$$L_1 = L - L_2 \tag{2.6}$$

thus

$$L^2 - 2LL_2 + L_2^2 = L_2^2 + D^2 - 2L_2 D\cos(\alpha_2 - \beta) \tag{2.7}$$

solving (2.7) for L_2 gives

$$L_2 = \frac{1}{2}\left(\frac{L^2 - D^2}{L - D\cos(\alpha_2 - \beta)}\right). \tag{2.8}$$

Differentiating Eq. (2.8) with respect to time gives

$$\dot{L}_2 = \gamma_1\dot{L} + \gamma_2\dot{D} + \gamma_3(\dot{\alpha}_2 - \dot{\beta}) \tag{2.9}$$

$$\ddot{L}_2 = \gamma_1\ddot{L} + \gamma_2\ddot{D} + \gamma_3(\ddot{\alpha}_2 - \ddot{\beta}) + f_2 \tag{2.10}$$

with the abbreviations

$$\gamma_1 = \frac{L^2 + D^2 - 2DL\cos(\alpha_2 - \beta)}{2[L - D\cos(\alpha_2 - \beta)]^2}$$

$$\gamma_2 = \frac{[L^2 + D^2]\cos(\alpha_2 - \beta) - 2DL}{2[L - D\cos(\alpha_2 - \beta)]^2}$$

$$\gamma_3 = -\frac{[D^3 - DL^2]\sin(\alpha_2 - \beta)}{2[L - D\cos(\alpha_2 - \beta)]^2}$$

$$f_2 = \dot{\gamma}_1\dot{L} + \dot{\gamma}_2\dot{D} + \dot{\gamma}_3(\dot{\alpha}_2 - \dot{\beta}) \tag{2.11}$$

2.3 Kinematics of the pulley

The global position of the pulley is described as

$$x_1 = x_C - L_2 \cos\alpha_2 \tag{2.12}$$
$$y_1 = y_C - L_2 \sin\alpha_2 \tag{2.13}$$

where x_C and y_C are the coordinates of the tip of the boom with respect to the Inertial reference frame. They can be represented as

$$x_C = x_A + (L_3 + L_4)\cos\beta \tag{2.14}$$
$$y_C = y_A + (L_3 + L_4)\sin\beta \tag{2.15}$$

with

$$x_A = x_G + L_5 \cos\delta$$
$$= x_{G_0} + L_5 \cos(\delta_0 + \Delta\delta) \tag{2.16}$$
$$y_A = y_G + L_5 \sin\delta$$
$$= y_G + L_5 \sin(\delta_0 + \Delta\delta) \tag{2.17}$$

where x_G represents an excitation in the x direction and y_G represents excitation in the y direction (Heave), and δ_0 represents the elevation angle of the base pivot of the crane with respect to the ship's roll center, and $\Delta\delta$ denotes the roll angle of the ship. Differentiating Eqs. (2.12, 2.13) to find the first and second derivative with respect to time yields

$$\dot{x}_1 = \dot{x}_C - \dot{L}_2 \cos\alpha_2 + L_2 \sin\alpha_2\dot{\alpha}_2 \tag{2.18}$$
$$\dot{y}_1 = \dot{y}_C - \dot{L}_2 \sin\alpha_2 - L_2 \cos\alpha_2\dot{\alpha}_2 \tag{2.19}$$

Where

$$\dot{x}_C = \dot{x}_A - (L_3 + L_4)\sin\beta\dot{\beta} \tag{2.20}$$
$$\dot{y}_C = \dot{y}_A + (L_3 + L_4)\cos\beta\dot{\beta} \tag{2.21}$$
$$\dot{x}_A = \dot{x}_G - L_5 \sin\delta\dot{\delta} \tag{2.22}$$
$$\dot{y}_A = \dot{y}_G + L_5 \cos\delta\dot{\delta} \tag{2.23}$$

The second derivative of Eqs.(2.18, 2.19) is given by

$$\ddot{x}_1 = \ddot{x}_C - \cos\alpha_2 \ddot{L}_2 + 2\sin\alpha_2 \dot{L}_2 \dot{\alpha}_2 + l_2(\sin\alpha_2 \ddot{\alpha}_2 + \cos\alpha_2 \dot{\alpha}_2^2) \tag{2.24}$$

$$\ddot{y}_1 = \ddot{y}_C - \sin\alpha_2 \ddot{L}_2 + 2\cos\alpha_2 \dot{L}_2 \dot{\alpha}_2 - L_2(\cos\alpha_2 \ddot{\alpha}_2 - \sin\alpha_2 \dot{\alpha}_2^2) \tag{2.25}$$

where

$$\ddot{x}_C = \ddot{x}_A - (L_3 + L_4)(\cos\beta\dot{\beta}^2 + \sin\beta\ddot{\beta}) \tag{2.26}$$

$$\ddot{y}_C = \ddot{y}_A + (L_3 + L_4)(-\sin\beta\dot{\beta}^2 + \cos\beta\ddot{\beta}) \tag{2.27}$$

$$\ddot{x}_A = \ddot{x}_O - L_5(\cos\delta\dot{\delta}^2 + \sin\delta\ddot{\delta}) \tag{2.28}$$

$$\ddot{y}_A = \ddot{y}_O + L_5(-\sin\delta\dot{\delta}^2 + \cos\delta\ddot{\delta}) \tag{2.29}$$

2.4 Kinematics of the payload

The global position of the payload is expressed as

$$x_2 = x_1 + l\sin\phi_2 \tag{2.30}$$

$$y_2 = y_1 - l\cos\phi_2 \tag{2.31}$$

this is differentiated to find the first and second derivative with respect to time to give

$$\dot{x}_2 = \dot{x}_1 + l\cos\phi_2\dot{\phi}_2 \tag{2.32}$$

$$\dot{y}_2 = \dot{y}_1 + l\sin\phi_2\dot{\phi}_2 \tag{2.33}$$

$$\ddot{x}_2 = \ddot{x}_1 + l\cos\phi_2\ddot{\phi}_2 - l\sin\phi_2\dot{\phi}_2^2 \tag{2.34}$$

$$\ddot{y}_2 = \ddot{y}_1 + l\cos\phi_2\dot{\phi}_2^2 + l\sin\phi_2\ddot{\phi}_2 \tag{2.35}$$

2.5 Overall equations of motion

To find the equation of motion of the system the team decided to use Lagrange method depending on the total kinetic energy and total potential energy of the system, because it is an easy direct method.

Lagrange method states

$$\frac{d}{dt}\left(\frac{\partial T}{\partial \dot{q}_j}\right)-\frac{\partial T}{\partial q_j}+\frac{\partial V}{\partial q_j}=Q_j \tag{2.36}$$

where

T : Total kinetic Energy.

V : Total potential energy.

q_j : Generalized coordinate, (here $q_1=\alpha_2$, $q_2=\phi_2$).

Q_j : Nonconservative generalized force.

where the value of generalized forces Q_j can be computed as follow

$$Q_j=\sum\left(F_{xk}\frac{\partial x_k}{\partial q_j}+F_{yk}\frac{\partial y_k}{\partial q_j}+F_{zk}\frac{\partial z_k}{\partial q_j}\right) \tag{2.37}$$

where F_{xk}, F_{yk}, and F_{zk} represents external forces acting on k_{th} mass in the x, y, and z directions respectively, and x_k, y_k, and z_k are displacements of k_{th} mass in the x, y, and z directions respectively.

The total kinetic energy of the system can be represented as

$$T = \frac{1}{2}m_1\left(\dot{x}_1^2 + \dot{y}_1^2\right) + \frac{1}{2}m_2\left(\dot{x}_2^2 + \dot{y}_2^2\right)$$

$$= \frac{1}{2}m_1\left(\dot{x}_1^2 + \dot{y}_1^2\right) + \frac{1}{2}m_2\left[\left(\dot{x}_1^2 + l\cos\phi_2\dot{\phi}_2\right)^2 + \left(\dot{y}_1^2 + l\sin\phi_2\dot{\phi}_2\right)^2\right]. \quad (2.38)$$

And the total potential energy of the system can be represented as

$$V = m_1 y_1 g + m_2 y_2 g$$

$$= m_1 y_1 g + m_2 g(y_1 - l\cos\phi_2). \quad (2.39)$$

Therefore to find equation of motion Lagrange's equation should be applied for both pulley and payload as follow

$$\frac{d}{dt}\left(\frac{\partial L}{\partial \dot{\alpha}_2}\right) - \frac{\partial L}{\partial \alpha_2} + \frac{\partial V}{\partial \alpha_2} = Q_1 \quad (2.40)$$

$$\frac{d}{dt}\left(\frac{\partial L}{\partial \dot{\phi}_2}\right) - \frac{\partial L}{\partial \phi_2} + \frac{\partial V}{\partial \phi_2} = Q_2 \quad (2.41)$$

where α_2 and ϕ_2 are the generalized coordinates for pulley and payload respectively.

2.5.1 Evaluation of Q_1 and Q_2

By substituting the appropriate values of F_{xk}, F_{yk}, F_{zk}, x_k, y_k, and z_k in Eq. (2.37) we can get Q_1 and Q_2 as

$$Q_1 = p_2(-\gamma_3\cos\alpha_2 + L_3\sin\alpha_2) \quad (2.42)$$

$$Q_2 = p_2 l\cos\phi_2. \quad (2.43)$$

2.5.2 Equation of motion of the pulley

Substituting Eqs. (2.38, 2.39, & 2.42) in Eq. (2.40), then the resulted nonlinear differential equation of the pulley expressed as

$$
\begin{aligned}
&M[L_2^2+\gamma_3^2]\ddot{\alpha}_2\\
&+m_2l\left[L_2s(\alpha_2-\phi_2)-\gamma_3c(\phi_2-\alpha_2)\right]\ddot{\phi}_2\\
&+M[-\gamma_3L_Bs(\alpha_2-\beta)-L_BL_2c(\alpha_2-\beta)-\gamma_3^2]\ddot{\rho}\\
&+M[\gamma_3\gamma_1]\ddot{L}\\
&+M[\gamma_3\gamma_2]\ddot{D}\\
&+M\left[-L_2L_Cc(\delta-\alpha_2)-L_2L_Bc(\alpha_2-\beta)-\gamma_3L_Cs(\alpha_2-\delta)-\gamma_3L_Bs(\alpha_2-\beta)-\gamma_3^2\right]\ddot{\delta}\\
&+M[L_2s\alpha_2-\gamma_2c\alpha_2]\ddot{x}_G\\
&-M[L_2c\alpha_2+\gamma_3s\alpha_2]\ddot{y}_G\\
&-M[L_2c\alpha_2+\gamma_3s\alpha_2]g\\
&+M\left[L_2L_Cs(\delta-\alpha_2)+\gamma_3L_Cc(\delta-\alpha_2)+L_2L_Bs(\beta-\alpha_2)+\gamma_3L_Bc(\alpha_2-\beta)\right]\dot{\delta}^2\\
&+M\left[L_2L_Bs(\beta-\alpha_2)+\gamma_3L_Bc(\alpha_2-\beta)\right]\dot{\rho}^2\\
&+m_2l\left[-L_2c(\phi_2-\alpha_2)+\gamma_3s(\phi_2-\alpha_2)\right]\dot{\phi}_2^2+M[L_2\gamma_3]\dot{\alpha}_2^2\\
&+M\gamma_3f_2-m_2lc(\alpha_2-\phi_2)\dot{\gamma}_3\dot{\phi}_2\\
&+m_2l[L_2c\phi_2s\alpha_2-L_2c\phi_2c\alpha_2]\dot{\phi}_2\dot{\alpha}_2\\
&+M\left[L_Cs(\alpha_2-\delta)+\gamma_3+L_Bs(\alpha_2-\beta)\right]\dot{\delta}\left(\frac{\partial\dot{L}_2}{\partial\alpha_2}-\dot{\gamma}_3\right)\\
&+M\left[\gamma_3+L_Bs(\alpha_2-\beta)\right]\dot{\rho}\left(\frac{\partial\dot{L}_2}{\partial\alpha_2}-\dot{\gamma}_3\right)+m_2lc(\phi_2-\alpha_2)\frac{\partial\dot{L}_2}{\partial\phi_2}\dot{\phi}_2\\
&+M\left[c\alpha_2\dot{X}_G+s\alpha_2\dot{Y}_G+\gamma_1\dot{L}+\gamma_2\dot{D}+\gamma_3\dot{\alpha}_2\right]\left(\frac{\partial\dot{L}_2}{\partial\alpha_2}-\dot{\gamma}_3\right)\\
&+2M[\gamma_1\dot{L}+\gamma_2\dot{D}-\gamma_3\dot{\rho}+\gamma_3\dot{\delta}]\dot{\alpha}_2\\
&=p_2[L_2s\alpha_2-\gamma_3c\alpha_2]
\end{aligned}
\tag{2.44}
$$

where s & c letters denotes sine & cosine functions respectively, L_B denotes the total boom length (L_3+L_4), and M is equal to the sum of the pulley and payload masses (M=m_1+m_2).

Chapter three

Linearization and state space representation

In chapter two, the nonlinear equations of the system (2.44 & 2.45) were obtained, and since we are interested in the linear model of the system, Eqs. (2.44 & 2.45) are to be linearized using Taylor series expansion, and then state space of linear system will be developed.

3.1 Linearization

Sometimes only the solutions of linear systems may be found explicitly. The problem is that general real life problems may only be modeled by nonlinear systems. What happens around an equilibrium point remains a mystery so far. Here we solved the problem, and the main idea is to approximate a nonlinear system by a linear one (around the equilibrium point) using Taylor series expansion. This decision comes after making sure that nonlinear terms has small negligible effects on the system [1].

In Taylor series expansion a nonlinear function $F(j_1, j_2, \ldots j_n)$ can be expressed as

$$F \approx F\big|_{O.P} + \sum_{i=1}^{n} \left.\frac{\partial F}{\partial j_i}\right|_{O.P} \Delta j_i + \textit{higher order terms} \qquad (3.1)$$

where O.P represents operating point (equilibrium point), which was derived in chapter one. A linear approximation can be obtained by neglecting the higher order terms.

Chapter three

Linearization and state space representation

In chapter two, the nonlinear equations of the system (2.44 & 2.45) were obtained, and since we are interested in the linear model of the system, Eqs. (2.44 & 2.45) are to be linearized using Taylor series expansion, and then state space of linear system will be developed.

3.1 Linearization

Sometimes only the solutions of linear systems may be found explicitly. The problem is that general real life problems may only be modeled by nonlinear systems. What happens around an equilibrium point remains a mystery so far. Here we solved the problem, and the main idea is to approximate a nonlinear system by a linear one (around the equilibrium point) using Taylor series expansion. This decision comes after making sure that nonlinear terms has small negligible effects on the system [1].

In Taylor series expansion a nonlinear function $F(j_1, j_2, \ldots j_n)$ can be expressed as

$$F \approx F\big|_{O.P} + \sum_{i=1}^{n} \left.\frac{\partial F}{\partial j_i}\right|_{O.P} \Delta j_i + higher\ order\ terms \qquad (3.1)$$

where O P represents operating point (equilibrium point), which was derived in chapter one. A linear approximation can be obtained by neglecting the higher order terms.

Then the linearized model corresponding to Eq. (2.44) can be expressed as

$$
\begin{aligned}
&+M[l_{20}^{2}+\gamma_{30}^{2}]\Delta\ddot{\alpha}_2\\
&+m_2 l[L_{20}s(\alpha_{20}-\phi_{20})-\gamma_{30}c(\phi_{20}-\alpha_{20})]\Delta\ddot{\phi}_2\\
&+M\left[-\gamma_{30}L_B s(\alpha_{20}-\beta_0)-L_B L_{20}c(\alpha_{20}-\beta_0)-\gamma_{30}^{2}\right]\Delta\ddot{\rho}\\
&+M[\gamma_{30}\gamma_{10}]\Delta\ddot{L}\\
&+M[\gamma_{30}\gamma_{20}]\Delta\ddot{U}\\
&+M\begin{bmatrix}-L_{20}L_5 c(\delta_0-\alpha_{20})-l_{20}l_B c(\alpha_{20}-\beta_0)\\ -\gamma_{30}L_5 s(\alpha_{20}-\delta_0)-\gamma_{30}l_B s(\alpha_{20}-\beta_0)-\gamma_{30}^{2}\end{bmatrix}\Delta\ddot{\delta}\\
&+M[l_{20}s\alpha_{20}-\gamma_{30}c\alpha_{20}]\Delta\ddot{x}_G\\
&-M[l_{20}c\alpha_{20}+\gamma_{30}s\alpha_{20}]\Delta\ddot{y}_G\\
&-Mg(k_{21}\sin\alpha_{20}+k_{22}\cos\alpha_{20})\Delta\rho\\
&-Mg(k_{11}\sin\alpha_{20}+k_{12}\cos\alpha_{20})\Delta L\\
&-Mg(k_{31}\sin\alpha_{20}+k_{32}\cos\alpha_{20})\Delta U\\
&-Mg(2\cos\alpha_{20}\gamma_{30}+(k_{41}-L_{20})\sin\alpha_{20})\Delta\alpha_2\\
&-Mg(k_{21}\sin\alpha_{20}+k_{22}\cos\alpha_{20})\Delta\delta\\
&-Mg[l_{20}c\alpha_{20}+\gamma_{30}s\alpha_{20}]\quad=\quad p_2[l_{20}s\alpha_{20}+\gamma_{30}c\alpha_{20}]
\end{aligned}
\tag{3.2}
$$

and the linearized model corresponding to Eq. (2.45) can be expressed as

$$
\begin{aligned}
&+m_2[\gamma_{30}c(\alpha_{20}-\phi_{20})-L_{B0}s(\beta_0-\phi_{20})]\Delta\ddot{\rho}\\
&-m_2\gamma_{10}c(\alpha_{20}-\phi_{20})\Delta\ddot{L}-m_2\gamma_{20}c(\alpha_{20}-\phi_{20})\Delta\ddot{U}\\
&+m_2[L_{20}s(\alpha_{20}-\phi_{20})-\gamma_{30}c(\alpha_{20}-\phi_{20})]\Delta\ddot{\alpha}_2\\
&+m_2[\gamma_{30}c(\alpha_{20}-\phi_{20})-L_B s(\beta_0-\phi_{20})+L_5 s(\phi_{20}-\delta_0)]\Delta\ddot{\delta}\\
&+m_2 l\Delta\ddot{\phi}_2+m_2 c\phi_{20}\Delta\ddot{x}_G+m_2 s\phi_{20}\Delta\ddot{y}_G+m_2 gc\phi_{20}\Delta\phi_2=p_2 c\phi_2
\end{aligned}
\tag{3.3}
$$

therefore the linear equation of motion of the whole system can be expressed in matrix form as

$$
\begin{bmatrix} M\left(L_{20}^2+\gamma_{30}^2\right) & m_2\begin{pmatrix} -l\gamma_{30}\cos(\phi_0-\alpha_{20}) \\ -lL_{20}\sin(\phi_0-\alpha_{20}) \end{pmatrix} \\ (m_2L_{20}\sin\alpha_{20}-m_2\gamma_{30}\cos\alpha_{20}) & m_2l \end{bmatrix} \begin{bmatrix} \Delta\ddot{\alpha}_2 \\ \Delta\ddot{\phi}_2 \end{bmatrix}
$$

$$
+\begin{bmatrix} -Mg\left(2\cos\alpha_{20}\gamma_{30}+(k_{21}-L_{20})\sin\alpha_{20}\right) & 0 \\ 0 & m_2g \end{bmatrix} \begin{bmatrix} \Delta\alpha_2 \\ \Delta\phi_2 \end{bmatrix} =
$$

$$
\begin{bmatrix} M\begin{pmatrix} -\gamma_{30}L_B\sin(\beta_0-\alpha_{20}) \\ +L_BL_{20}\cos(\beta_0-\alpha_{20})+\gamma_{30}^2 \end{pmatrix} & M\gamma_{10}\gamma_{30} & -M\gamma_{20}\gamma_{30} \\ (m_2L_B\sin\beta_0-m_2\gamma_{30}\cos\alpha_{20}) & m_2\gamma_{10}\cos\alpha_{20} & m_2\gamma_{20}\cos\alpha_{20} \end{bmatrix} \begin{bmatrix} \Delta\ddot{\rho} \\ \Delta\ddot{L} \\ \Delta\ddot{D} \end{bmatrix}
$$

$$
+\begin{bmatrix} M\begin{pmatrix} \gamma_{30}L_B\sin(\beta_0-\alpha_{20})-L_BL_{20}\cos(\beta_0-\alpha_{20}) \\ -\gamma_{30}L_5\sin(\delta_0-\alpha_{20})+L_5L_{20}\cos(\delta_0-\alpha_{20})-\gamma_{30}^2 \end{pmatrix} \\ (m_2L_5\sin\delta_0+m_2\gamma_{30}\cos\alpha_{20}-m_2L_B\sin\beta_0) \end{bmatrix} \Delta\ddot{\delta}
$$

$$
+\begin{bmatrix} R_1 & R_2 & R_3 \\ 0 & 0 & 0 \end{bmatrix} \begin{bmatrix} \Delta\rho \\ \Delta L \\ \Delta D \end{bmatrix}
$$

$$
+\begin{bmatrix} -Mg(k_{21}\sin\alpha_{20}+k_{22}\cos\alpha_{20}) \\ 0 \end{bmatrix} \Delta\delta
$$

$$
+\begin{bmatrix} M(\gamma_{30}\cos\alpha_{20}-L_{20}\sin\alpha_{20}) & M(\gamma_{30}\sin\alpha_{20}+L_{20}\cos\alpha_{20}) \\ -m_2 & 0 \end{bmatrix} \begin{bmatrix} \Delta\ddot{x}_G \\ \Delta\ddot{y}_G \end{bmatrix}
$$

$$
+\begin{bmatrix} (-\gamma_{20}\cos\alpha_{20}+L_{20}\sin\alpha_{20}) \\ 1 \end{bmatrix} p_2 \qquad (3.4)
$$

with

$$
K_{11}=\frac{\partial\gamma_3}{\partial L},\ K_{12}=\frac{\partial L_2}{\partial L}=\gamma_{10},\ K_{21}=\frac{\partial\gamma_3}{\partial\beta},\ K_{22}=\frac{\partial L_2}{\partial\beta}=-\gamma_{30}
$$

$$
K_{31}=\frac{\partial\gamma_3}{\partial D},\ K_{32}=\frac{\partial L_2}{\partial D},\ K_{41}=\frac{\partial\gamma_3}{\partial\alpha_2}=-K_{21}
$$

$$
R_1=Mg(k_{21}\sin\alpha_{20}+k_{22}\cos\alpha_{20})
$$

$$
R_2=Mg(k_{11}\sin\alpha_{20}+k_{12}\cos\alpha_{20})
$$

$$
R_3=Mg(k_{31}\sin\alpha_{20}+k_{32}\cos\alpha_{20}) \qquad (3.5)
$$

3.2 State space representation

The classical control theory and methods (such as root locus) are based on a simple input-output description of the plant, usually expressed as a transfer function. These methods do not use any knowledge of the interior structure of the plant, and limit us to single-input single-output (SISO) systems, and allows only limited control of the closed-loop behavior when feedback control is used. Modern control theory solves many of the limitations by using a much "richer" description of the plant dynamics. The so-called state-space description provide the dynamics as a set of coupled first-order differential equations in a set of internal variables known as *state variables*, together with a set of algebraic equations that combine the state variables into physical output variables.

The obtained linear equation of motion (3.4) can be written as

$$M_0\ddot{q} - B_1\ddot{u} - B_2\Delta\ddot{\delta} - B_3\ddot{x}_G = K_0 q + B_2 u + B_4\Delta\delta + B_6 x_G + B_7 p_2 , \tag{3.6}$$

to obtain the state space model for the above equation, let

$$z_1 = M_0 q - B_1 u - B_2\Delta\delta - B_5 x_G \tag{3.7}$$

$$z_2 = M_0\dot{q} - B_1\dot{u} - B_2\Delta\dot{\delta} - B_5\dot{x}_G \tag{3.8}$$

then the state space equations, corresponding to the current equilibrium point, can be expressed in vector form as

$$\dot{z} = Az + Bu + E\Delta\delta + Fx_G + Np_2 \tag{3.9}$$

where

$$z = [z_1 \quad z_2]^T \tag{3.10}$$

denotes the state vector of order 4×1, and

$$A=\begin{bmatrix} 0 & I \\ -K_0M_0 & 0 \end{bmatrix} \tag{3.11}$$

$$B=\begin{bmatrix} 0 \\ B_3-K_0M_0^{-1}B_1 \end{bmatrix} \tag{3.12}$$

represent the corresponding system and input matrices respectively, and

$$E=\begin{bmatrix} 0 \\ B_4-K_0M_0^{-1}B_2 \end{bmatrix} \tag{3.13}$$

$$N=\begin{bmatrix} 0 \\ B_7 \end{bmatrix} \tag{3.14}$$

$$F=\begin{bmatrix} 0 \\ B_6-K_0M_0^{-1}B_5 \end{bmatrix} \tag{3.15}$$

represent the disturbance matrices due to ship rolling, ship motion in the x and y directions, and disturbance force acting on the payload respectively. Here M_0 is assumed to be non-singular.

In view of Eqs. (3.2, 3.3), the initial conditions of the states can be expressed as

$$\begin{aligned} z(0)=&\begin{bmatrix} M_0 & 0 \\ 0 & M_0 \end{bmatrix}\begin{bmatrix} q(0) \\ \dot{q}(0) \end{bmatrix}-\begin{bmatrix} B_1 & 0 \\ 0 & B_1 \end{bmatrix}\begin{bmatrix} u(0) \\ \dot{u}(0) \end{bmatrix} \\ &-\begin{bmatrix} B_2 & 0 \\ 0 & B_2 \end{bmatrix}\begin{bmatrix} \Delta\delta(0) \\ \Delta\dot{\delta}(0) \end{bmatrix}-\begin{bmatrix} B_5 & 0 \\ 0 & B_5 \end{bmatrix}\begin{bmatrix} x_G(0) \\ \dot{x}_G(0) \end{bmatrix} \end{aligned} \tag{3.16}$$

The displacement vector q can be obtained from Eq. (3.2) as

$$\begin{aligned} q=&M_0^{-1}z_1+M_0^{-1}B_1u+M_0^{-1}B_2\Delta\delta+M_0^{-1}B_5x_G \\ &-[M_0^{-1}\quad 0]z+M_0^{-1}B_1u+M_0^{-1}B_2\Delta\delta+M_0^{-1}B_5x_G. \end{aligned} \tag{3.17}$$

System output can be written as

$$y = Cz + Du + E_0 \Delta\delta + F_0 x_0 \tag{3.18}$$

where

$$C = [M_0^{-1} \;\; 0] \tag{3.19}$$

is the output matrix, and

$$D = M_0^{-1} B_1 \tag{3.20}$$

$$E_0 = M_0^{-1} B_2 \tag{3.21}$$

$$F_0 = M_0^{-1} B_3 \tag{3.22}$$

represent the input and disturbances ($\Delta\delta$, x_0) direct transmission matrices respectively. Here the rolling motion of the ship $\Delta\delta$ is assumed to be measured. When we linearized the nonlinear system the coefficients of y_G became zeros which means y_G has no effect on the ship crane system in linear operations, but it has small effect in nonlinear operation.

3.3 Simulation results for the linear system

Simulation of the linear system is performed using MATLAB program, this is done by writing m-file and building a simulink model that represents the linear model as in Fig. (3.1).

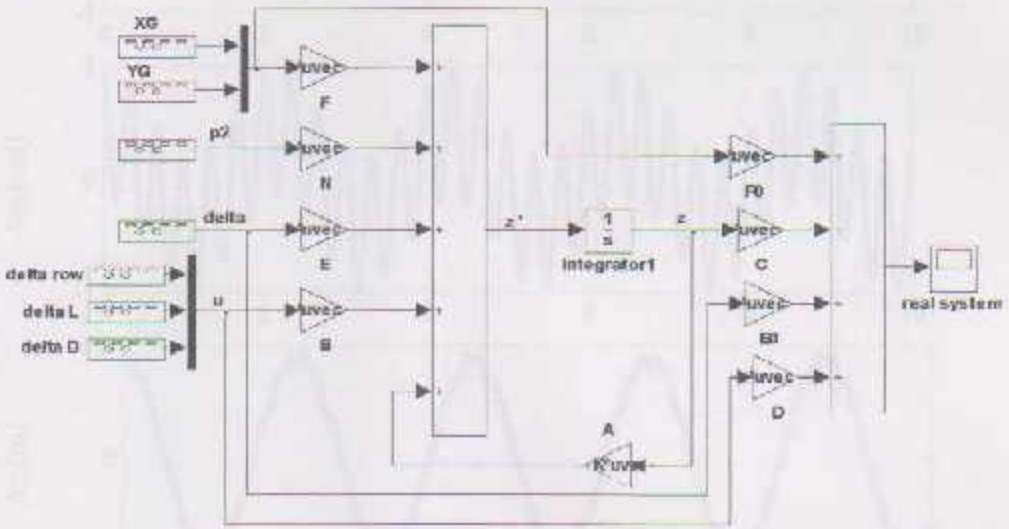

Figure (3.1): simulink model for the real system

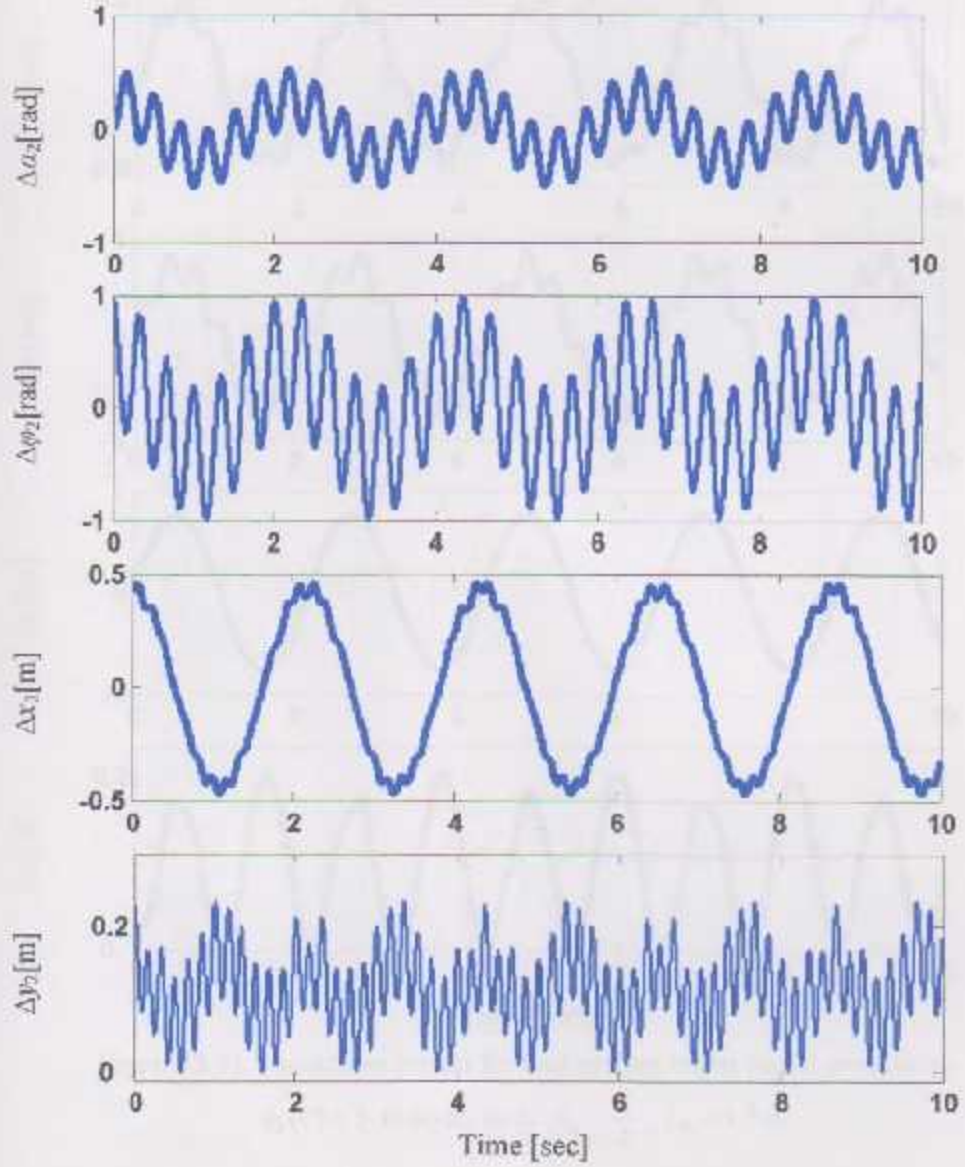

Figure (3.2): simulation results for real system under initial conditions $\phi_2(0)=1$ rad, with $\rho_0=-\frac{\pi}{4}$, $l_{c0}=1.5m$

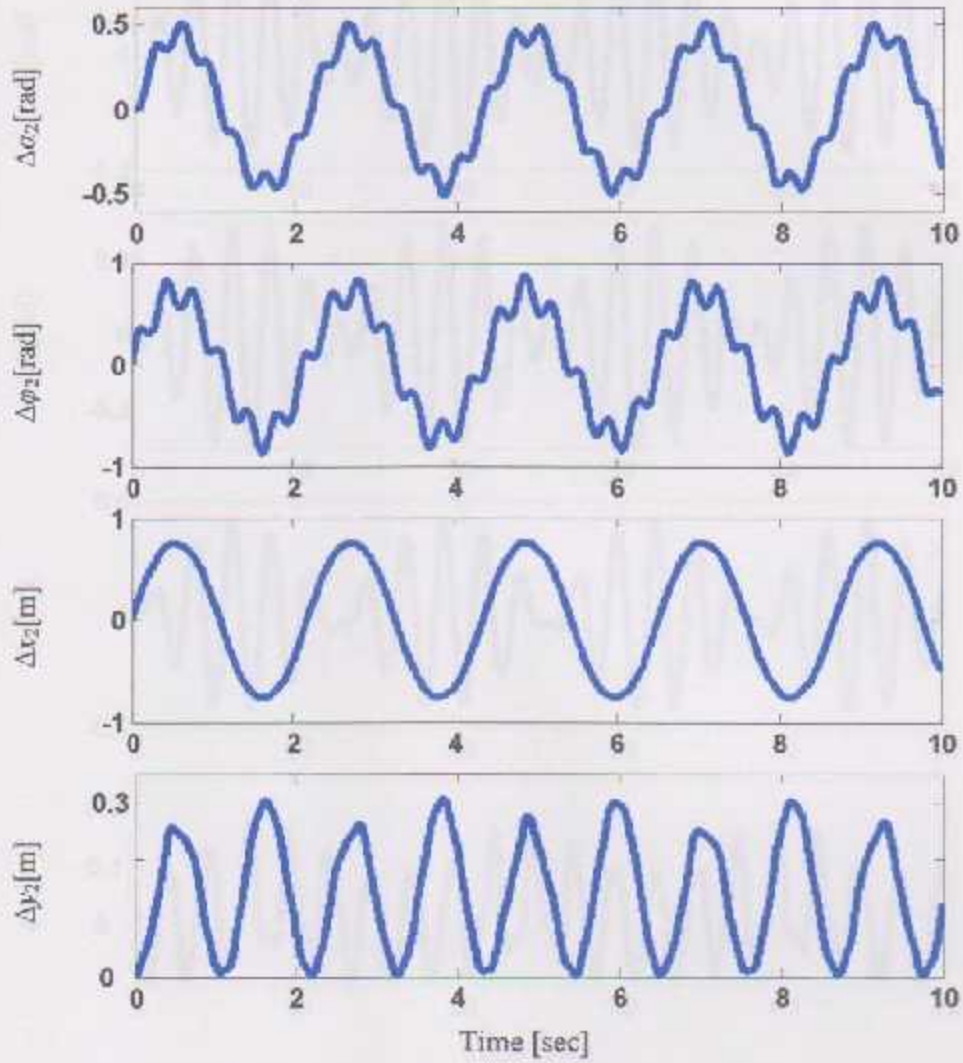

Figure (3.3): simulation results for real system under initial conditions $\dot{\phi}_2(0) = 5$ rad/sec, with $\rho_0 = \frac{\pi}{4}$, $L_0 = 1.5\,m$

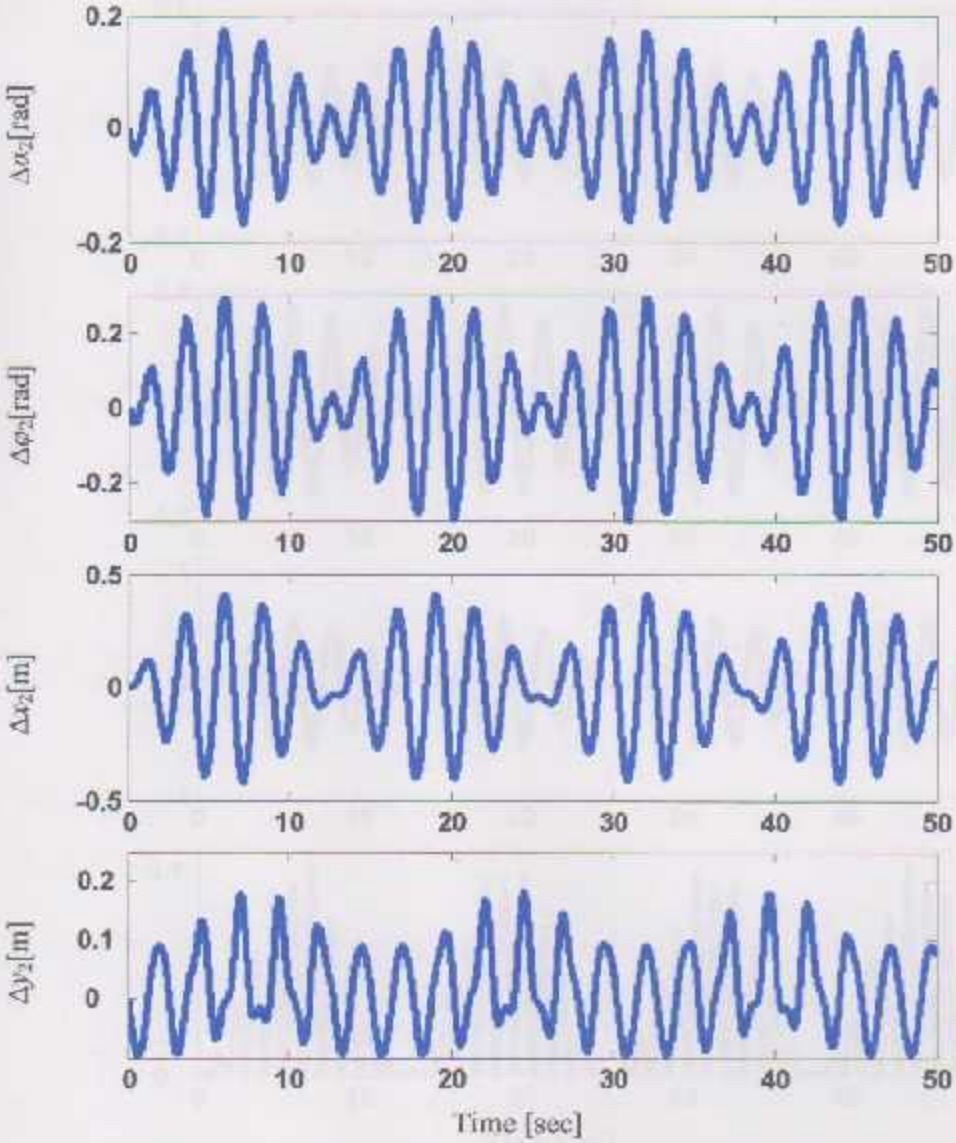

Figure (3.4): simulation results for real system under rolling effect $\Delta\delta = 3^{\circ}$, and frequency close to the eigenfrequency with $\rho_0 = \frac{\pi}{4}$, $l_0 = 1.5m$

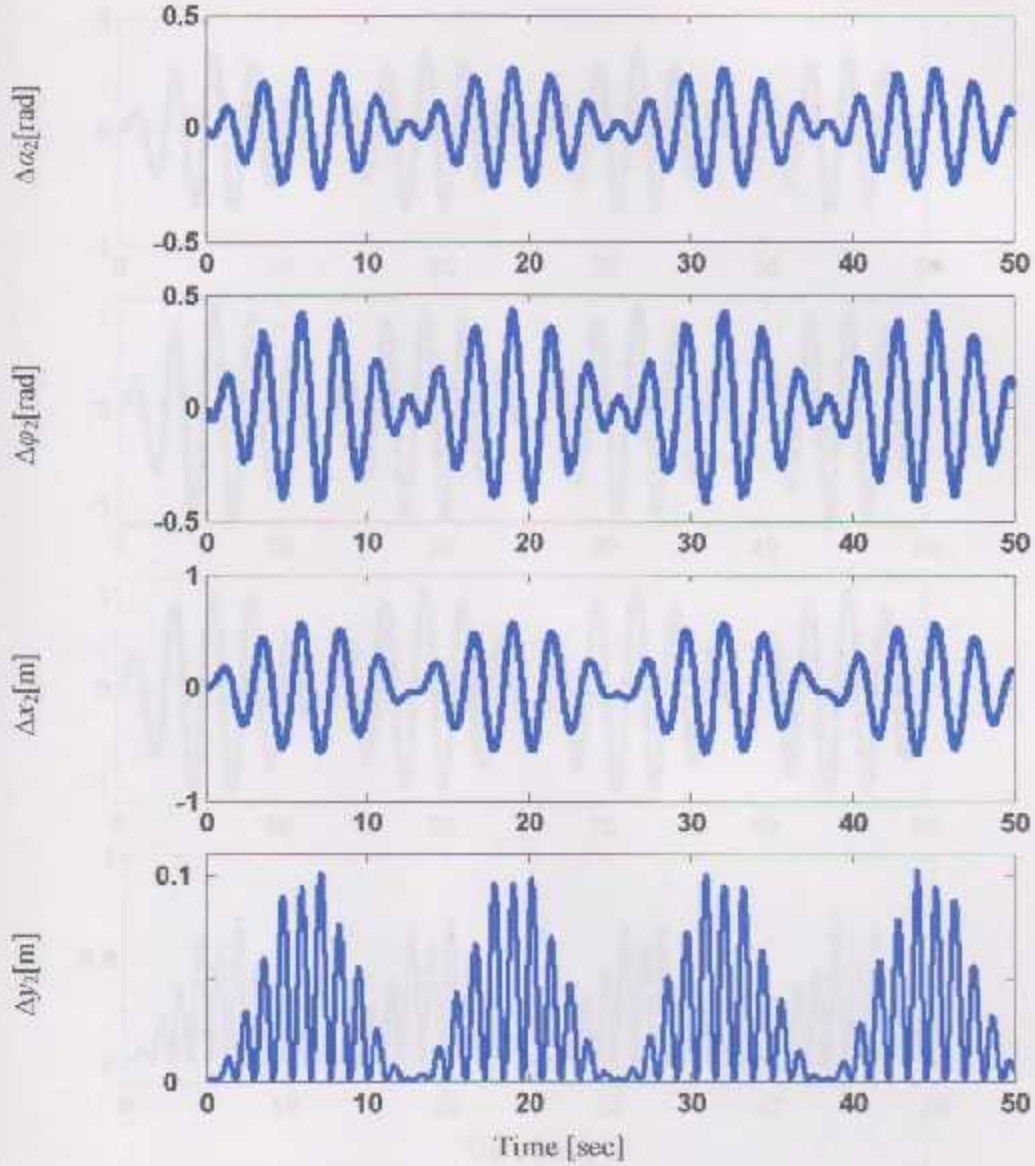

Figure (3.5): simulation results for real system under the effect of displacement $\Delta x_{01} = 10\ cm$, with frequency close to the eigenfrequency, $\rho_{02} = \frac{\pi}{4}$, $l_{02} = 1.5\,m$

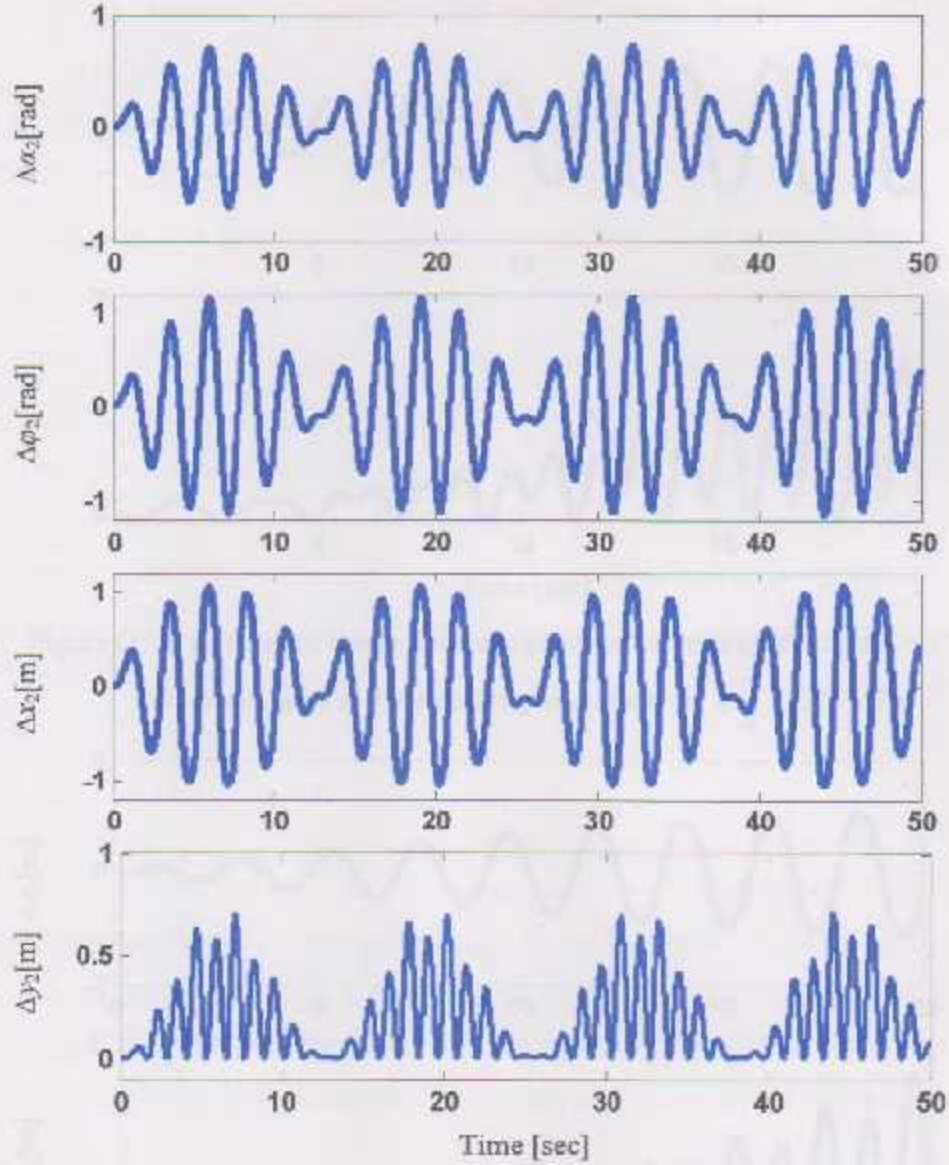

Figure (3.6): simulation results for real system under the effect of wind force $p_2 = 10\ N$, with frequency close to the eigenfrequency, $\rho_0 = \frac{\pi}{4}$, $L_0 = 1.5\,m$

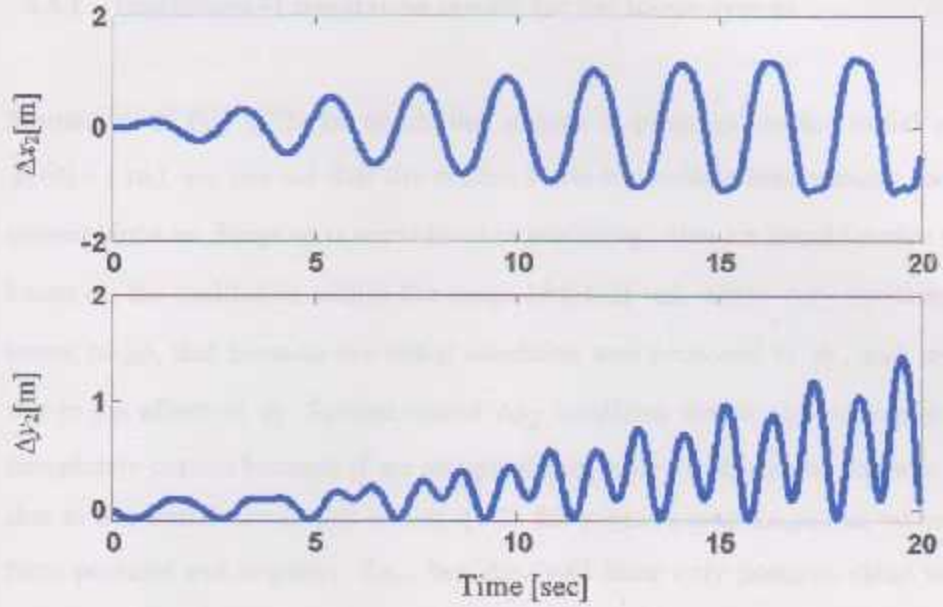

Figure (3.7): simulation results for real system under rolling effect $\Delta\delta = 3^{\circ}$, and frequency equal to the eigenfrequency with $\rho_0 = \frac{\pi}{4}$, $L_0 = 1.5m$

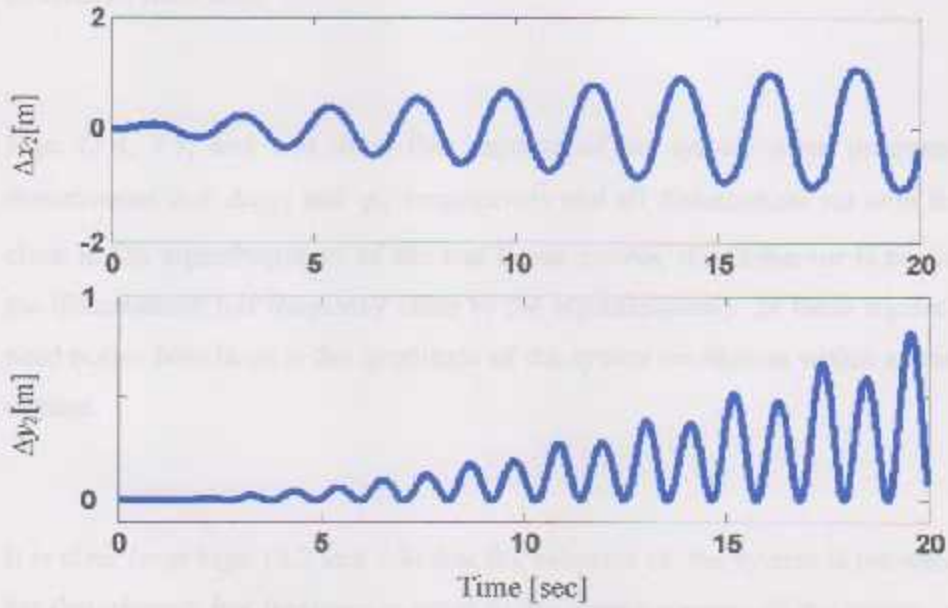

Figure (3.8): simulation results for real system under the effect of displacement $\Delta x_0 = 10\ cm$, with frequency equal to the eigenfrequency, $\rho_0 = \frac{\pi}{4}$, $L_{20} = 1.5m$

3.3.1 Discussion of simulation results for the linear system

Starting with Fig. (3.2) in which the system is proposed to the initial condition $\phi_2(0) = 1$ rad, we can see that the system starts to oscillate continuously, and this is correct since no damping is considered in modeling. Also we should notice that $\Delta\phi_2$ keeps on the oscillation within the range of [-1 1] rad, while $\Delta\alpha_2$ oscillates within lower range, that because the initial condition was proposed to ϕ_2, and α_2 moved due to the effect on ϕ_2. System output Δy_2 oscillates within positive range which is completely correct because if we imagined that pulley and payload starts to oscillate due to the initial conditions in Fig. (1.2) the payload with (x_2, y_2) as reference will have positive and negative Δx_2, but Δy_2 will have only positive value because it moves up the reference and return back to reference then move up again. In Fig. (3.3) the initial condition is velocity given for ϕ_2 then system outputs must start oscillation from zero.

Figs. (3.4, 3.5, and 3.6) show the response of the system when proposed to the disturbances $\Delta\delta$, Δx_G, and p_2 respectively and all disturbances act with frequency close to the eigenfrequency of the real linear system, the behavior is beating since the disturbances has frequency close to the eigenfrequency. In these figures we just need notice how large is the amplitude of the system oscillation within a small range of time.

It is clear from Figs. (3.7 and 3.8) that the behavior of the system is resonance since the disturbances has frequencies equal to the eigenfrequency of the system, and thus perform the extreme dangerous on the system.

Also from the simulation results of the linear real system we can ensure that the mathematical model of the linear real system is correct, since it gives reasonable response of the system for all effects that acted on it. By this conclusion we can move to the next step which is the controller design.

Chapter Four

Control system design

This chapter presents the observer and controller design in order to minimize the oscillation of the payload which can be induced from ship rolling or from any other disturbance that can act on the crane during the cargo transfer operation. When the frequency of the ship rolling or any other disturbance is close to the eigenfrequency of the crane for a period of time, resonance will occur and the oscillation of the payload can grow to a dangerous level even with small amplitude of the disturbance. This means that, if no control is used, the operation of the crane should be suspended. This control problem is explained in detail in this chapter.

4.1 Test for controllability and observability

Before starting with the controller design, one must check the controllability. A linear system is said to be completely controllable if, for all initial times t_0 and all initial states $z(t_0)$, there exists some input function that drives the state vector to any final state $z(t_1)$ at some finite time $t_1 > t_0$. Controllability of the system is determined by matrices $\boldsymbol{A}$ and $\boldsymbol{B}$.

4.1.1 Controllability test

There are different tests to check the controllability of a physical system. Here we will use the controllability matrix to determine system controllability, where the controllability matrix of a linear system is defined as

$$C = [B \;\; AB \;\; A^2B \ldots A^{n-1}B] \tag{4.1}$$

where n is the dimension of matrix A, here controllability matrix must have full row rank so the system to be controllable.

If we return to the ship crane model, the rank of C should be four, to ensure full state controllability of the crane. Because we have four states; two states for position and another two states for velocity, applying this method to the crane model results in

$$\text{Rank}[B \;\; AB \;\; A^2B \;\; A^3B] = \dim(z) = 4 \tag{4.2}$$

which means that the system is completely controllable, and the state feedback compensation method (state feedback control) can be used to control the whole system.

Before starting with the design of a controller we must be sure, with the availability of all states, here we have two available (measured) states, using two rotary sensors for $\Delta\alpha_2$ and $\Delta\phi_2$. To avoid buying another expensive two sensors to measure the velocities we will design a mathematical model called estimator (observer) which estimates the two velocity states, and extends the model to estimate also the unknown disturbances.

4.1.2 Observability test

Analogously, a linear system is said to be completely observable if, for all initial times t_0, the state vector $z(t_0)$ can be determined from the output function, defined over a finite time $t_1 > t_0$. Consequently, observability involves the matrices A and C.

Always before starting with the observer design, we should check the observability of the system, by finding the rank of the observability matrix that defined as

$$O = \begin{bmatrix} C \\ CA \\ CA^2 \\ \vdots \\ CA^{n-1} \end{bmatrix} \tag{4.3}$$

and it must has full rank (rank (O) n) for an observable system. Applying this test on the ship crane model we will get

$$\text{Rank} \begin{bmatrix} C \\ CA \\ CA^2 \\ CA^3 \end{bmatrix} = 4 \tag{4.4}$$

This means the system is observable, or we can determine the state vector from the output function, we have all states available by using this estimator to estimate all states.

4.2 Control system design

In order to design a state feedback controller two methods can be used pole placement, and optimal method. Pole placement is required to assume the poles anywhere in the left half plane, but always in this method, we have a problem in identifying the desired locations of the controller poles. As a hint the location of the poles of the observer should be further to the left of the controller poles, we will not use this method to design a controller, but we will use another method called optimal method, which depends on minimizing of the energy equation

$$\int \left(x^T Q x + u^T R u \right) dt. \tag{4.5}$$

where Q and R are symmetric positive definite weighting matrices for the states and the inputs respectively [17].

4.3 State and disturbance estimation

For the design of an optimal state feedback controller, all state variables must be available. In most cases, as it is seen in the ship crane under consideration, not all the state variables are measured since the required sensors are not available due to economic or practical reasons. Only 2 out of 4 states can be easily measured. In order to reconstruct the entire state vector z, a suitable observer can be designed as a first step to realize optimal state controller design if the related conditions for applications are fulfilled. Since the state space model of the crane contains the unknown disturbance force p_2, and unknown disturbance x_G (sea motion in the x-direction), the state variables and the unknown disturbances can be estimated by using a special observer design able to reconstruct system states in presence of additional unknown effects acting on the system. Here a Proportional-Integral Observer (PI-Observer) is used. The structure of this Observer is shown in Figs. (4.1 & 4.2). The estimated states are represented by the equations

$$\dot{\hat{z}} = A\hat{z} + Bu + E\Delta\delta + F\hat{x}_G + N\hat{p}_2 + L_1(y_m - \hat{y}_m) \tag{4.6}$$

and the unknown disturbances are reconstructed by

$$\dot{\hat{p}}_2 = G_1\hat{p}_2 + L_3(y_m - \hat{y}_m) \tag{4.7}$$

$$\dot{\hat{x}}_G = G_2\hat{x}_G + L_2(y_m - \hat{y}_m) \tag{4.8}$$

where $\hat{y}_m$ is the output of the observer, L_1, L_2 and L_3 are the observer gain matrices of appropriate dimensions. Due to the difficulty of finding a simple linear

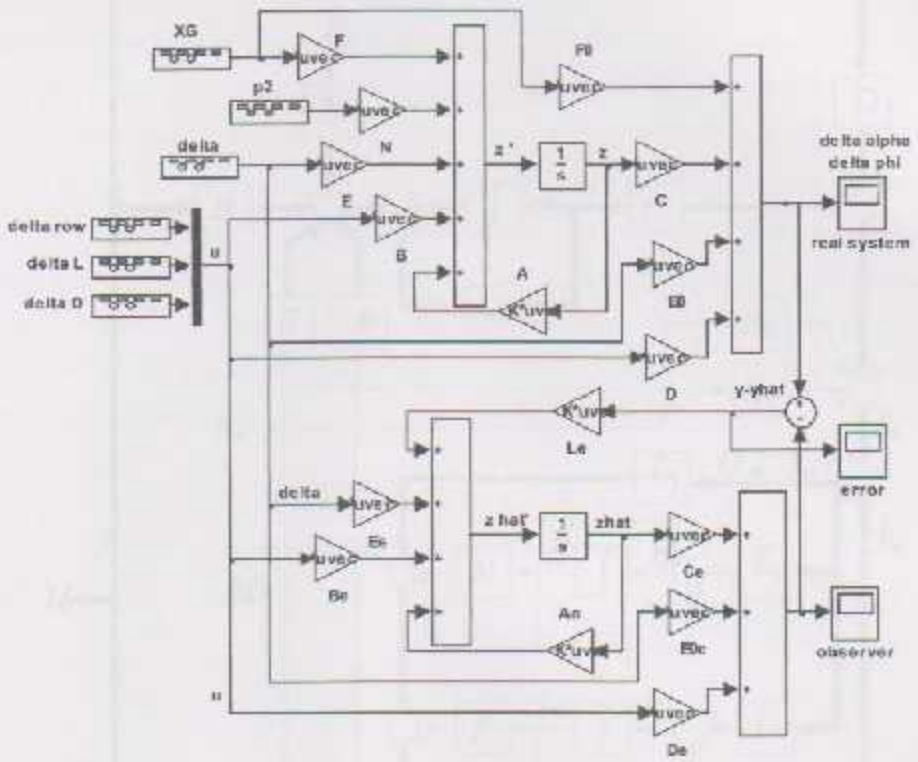

Figure (4.1): Simulink structure of the PI-Observer corresponding to the crane linear model

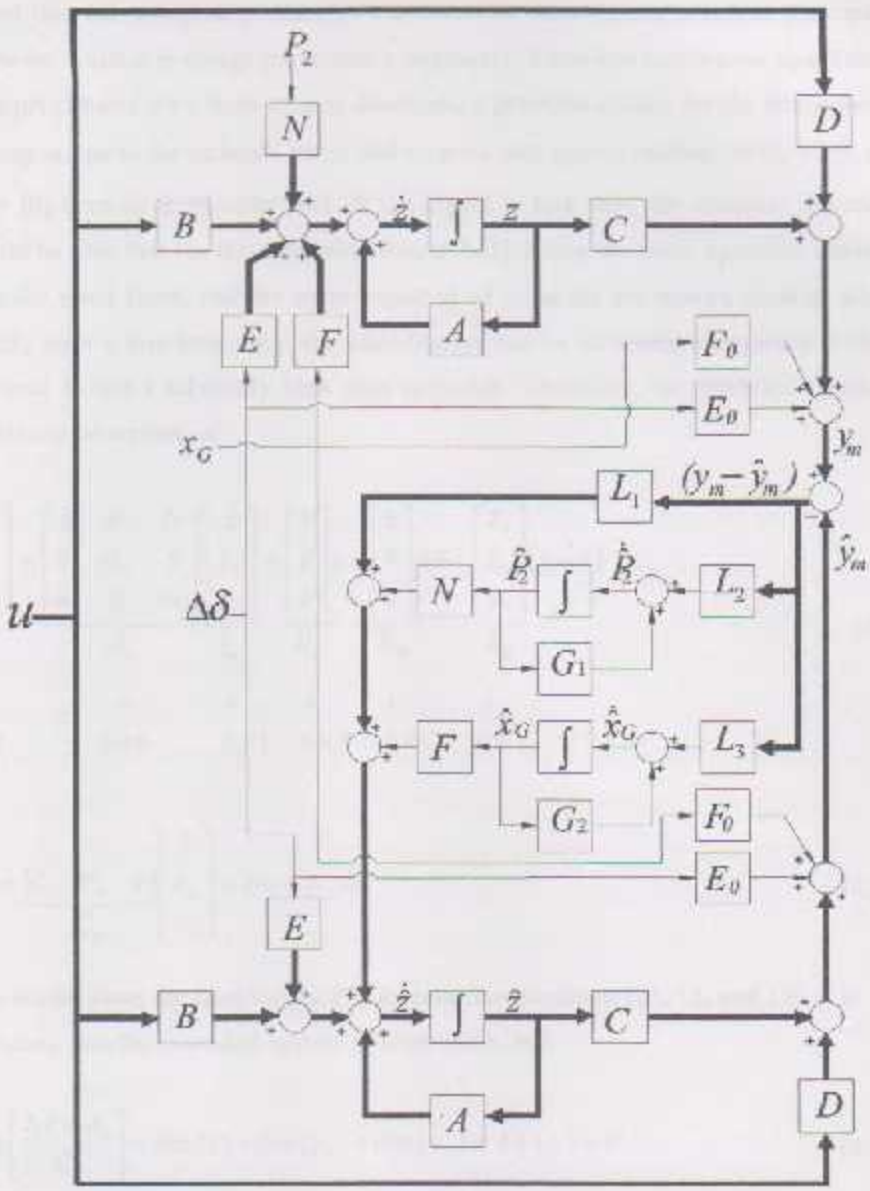

Figure (4.2): Structure of the PI-Observer corresponding to the crane linear model

model that can adequately describe the unknown disturbance, which is principally unknown, a suitable design procedure is necessary. Since any continuous signal can be approximated by a train of step functions, a practical choice for the linear model corresponding to the estimate of p_2 and x_G are a step approximation, or $G_1 = [0]$, and $G_2 = [0]$ here G_i is of order 1×1. If the signal is fast, then the observer dynamics should be also fast for the approximation to hold. Since the main expected cause of p_2 is the wind force, and the main expected of x_G is the see wave's motion, which usually have a low frequency, the disturbances can be estimated adequately without the need to use a relatively high gain approach. Therefore, the modified extended model can be written as

$$\underbrace{\begin{bmatrix}\dot{z}\\ \dot{x}_G\\ \dot{p}_2\end{bmatrix}}_{\dot{z}_e} = \underbrace{\begin{bmatrix}A & F & N\\ 0 & G_2 & 0\\ 0 & 0 & G_1\end{bmatrix}}_{\breve{A}_e}\underbrace{\begin{bmatrix}z\\ \hat{x}_G\\ \hat{p}_2\end{bmatrix}}_{\hat{z}_e} + \underbrace{\begin{bmatrix}B\\ 0\\ 0\end{bmatrix}}_{B_e}u + \underbrace{\begin{bmatrix}E\\ 0\\ 0\end{bmatrix}}_{E_e}\Delta\delta + \underbrace{\begin{bmatrix}L_1\\ L_2\\ L_3\end{bmatrix}}_{L_e}(y-\hat{y}) \tag{4.9}$$

$$\downarrow \qquad \downarrow \qquad \downarrow \quad \downarrow \quad \downarrow \quad \downarrow$$

$$6\times1 \qquad 6\times6 \qquad 6\times1 \quad 6\times3 \quad 6\times1 \quad 6\times2$$

$$\hat{y}_m = \underbrace{\begin{bmatrix}C & F_0 & 0\end{bmatrix}}_{\breve{C}_e}\begin{bmatrix}\hat{z}\\ \hat{x}_G\\ \hat{p}_2\end{bmatrix} + Du + E_0\Delta\delta \tag{4.10}$$

This model gives the base for the PI-Observer development [22, 12, and 13]. It is necessary that the extended system is observable, and

$$\operatorname{rank}\begin{bmatrix}\lambda_i I - A_e\\ C_e\end{bmatrix} = \dim(z) + \dim(p_2) + \dim(x_G) = 4+1+1-6 \tag{4.11}$$

is satisfied for all eigenvalues λ_i of the system. The error dynamics of the extended observer can be expressed by

$$\dot{e} = (A_e - L_e C_e)e - J\begin{bmatrix} \dot{x}_G \\ \dot{p}_2 \end{bmatrix} \tag{4.12}$$

where

$$e = \begin{bmatrix} z \\ p_2 \\ x_G \end{bmatrix} - \begin{bmatrix} \hat{z} \\ \hat{p}_2 \\ \hat{x}_G \end{bmatrix} \tag{4.13}$$

denotes the error vector of the extended observer, and

$$J = \begin{bmatrix} 0 \\ I_{2n2} \end{bmatrix} \tag{4.14}$$

represents an input matrix to the error equation. It can be seen from Eq. (4.12) that p_2 and x_G tend to produce a nonzero steady state error vector. This tendency is considerable if the disturbances signal coming from the wind and sea waves represents a fast dynamics. In reality, sea waves motion and wind effects acting as disturbances usually have low frequencies, which means that the effect of their time derivative on the error equation is not significant especially if the eigenvalue of the error equation corresponding to the estimated disturbance is very fast in comparison to the remaining eigenvalues. There are many different design techniques used to design the observer gain matrices. Here the gains are found by minimizing a linear quadratic performance index, which leads to solving the algebraic

$$A_e P + P A_e^T + Q_e - P C_e^T R_e^{-1} C_e P = 0, \tag{4.15}$$

The gain matrix of the observer is calculated by

$$L_e = P C_e^T R_e^{-1} \tag{4.16}$$

where Q_e and R_e are symmetric positive definite weighting matrices for the extended states and the measurements respectively.

One important point to be mentioned here is that the estimation error corresponding to the last two states (disturbances) has to be weighted much more than the other 4 states, i.e. the observer eigenvalues corresponding to last two states should be far to the left of the other eigenvalues in the complex plane. All other eigenvalues are weighted such that the observer is asymptotically stable and sufficiently faster than the real passive system. This guarantees that the observer error converges to zero in real time, which means that the estimates converge to their real values in real time and are ready for the implementation of an optimal state feedback controller; this strategy is successfully used for fault diagnosis of large systems [22] and other engineering applications [23,12].

Simulation results for an actual disturbance signals p_2 and x_G in addition to the actual displacements $(\Delta\alpha_2, \Delta\phi_2)$ are shown together with their estimation values in Fig. (4.3). Here the results are based on the dimensions of a scaled test rig boom length=3m, $I_2 = 0.5\,m$, $l = 0.5\,m$, $\delta_0 = \frac{\pi}{2}$, $m_2 = 5\,kg$ subjected to the disturbance force p_2 and x_G with nonzero initial condition. The initial conditions of the observer are set to zero and the actual initial condition vector of the original system is characterized by $\phi_2(0) = 30°$. Note that the error of the observer due to the difference in the initial conditions will appear in the first second, and the observer estimates the disturbance and the states very well. In Fig. (4.4), the payload is subjected to a disturbance force and disturbance x_G of variable frequency, it can also be noted that the observer gives an acceptable estimation of the disturbances.

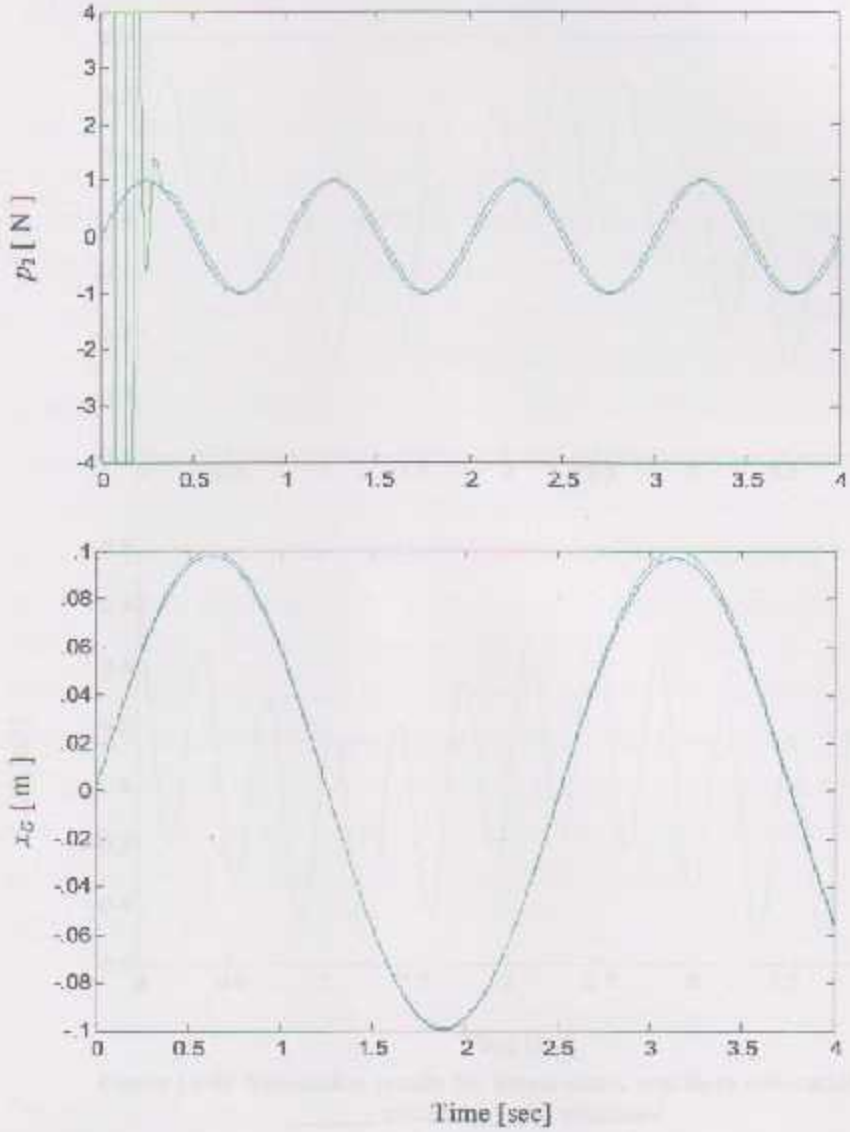

Figure (4.3): Simulation results for actual disturbances and there estimation

_____ actual _____ estimated

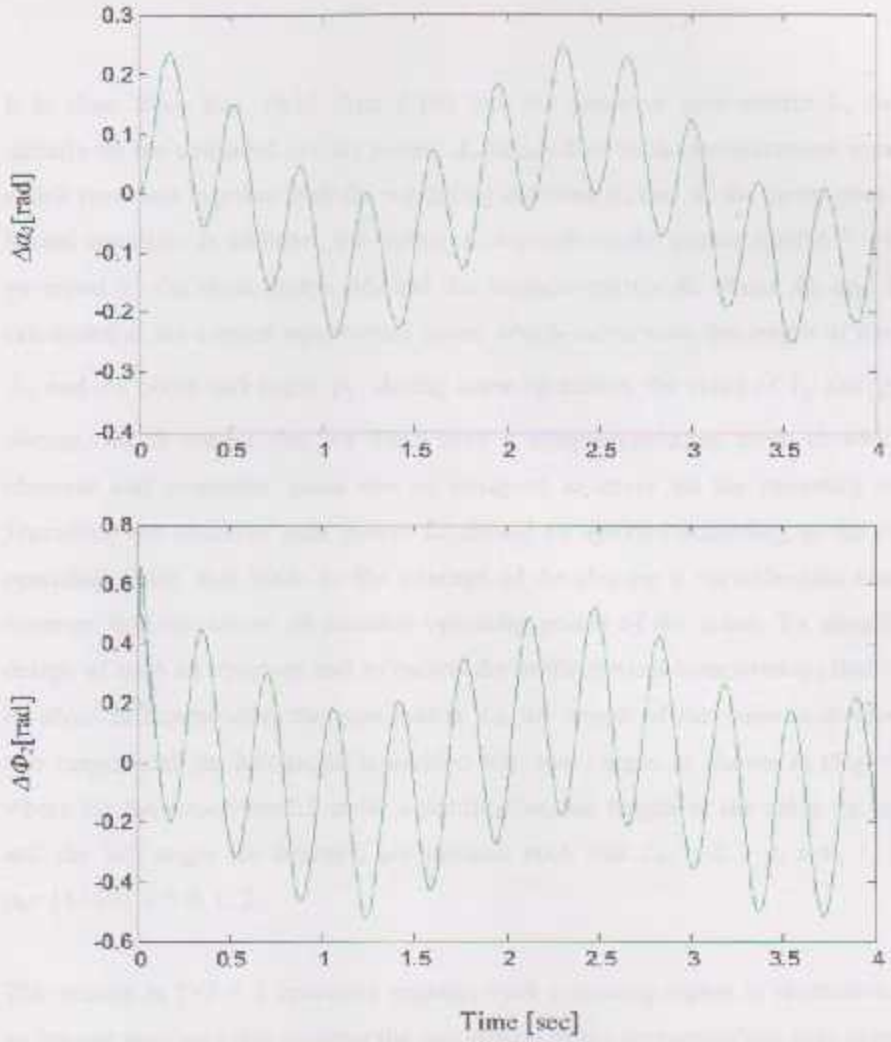

Figure (4.4): Simulation results for actual states and there estimation

_____ actual _____ estimated

4.4 Variable model problem

It is clear from Eqs. (4.15 And 4.16) that the observer gain matrix L_e depends directly on the extended system matrix A_e in addition to the measurement matrix C_e which represent together with the weighting matrices Q_e and R_e the parameters of the Ricatti equation. In addition, the matrix A_e depends on the system matrix A which is governed by the mass matrix M_θ and the stiffness matrix K_θ. Since M_θ and K_θ are calculated at the current equilibrium point, which varies with the length of the cable L_c and the boom luff angle ρ_0, during crane operation, the value of L_0 and ρ_0 will change, which means that we don't have a unique operating point at which the observer and controller gains can be designed to cover all the operating region. Therefore, the observer gain matrix L_e should be updated according to the current operating point, this leads to the concept of developing a variable-gain extended observer that can cover all possible operating points of the crane. To simplify the design of such an observer and to reduce the mathematical computations that can be involved in regenerating the gain matrix L_e, the length of the cable is divided into two ranges and the luff angle is divided into two ranges as shown in (Fig. 4.5.a), where for the scaled model under consideration, the length of the cable (in meters) and the luff angle (in degrees) are divided such that $L_{0_1} = 1 + r$, r=0, 1, 2 and $\rho_{0_2}=15+30s$, $s = 0, 1, 2$.

This results in $2\times2 = 4$ operating regions; each operating region is characterized by an integer number i that governs the calculation of the corresponding gain matrix L_e. This yields that, the operation of the crane is covered by different observer gain matrices L_{ei}. The switching between these gains takes place automatically according to the output i of the region finder Fig. (4.6), which uses the measurements of the luff angle and the length of the cable to detect the current operating region.

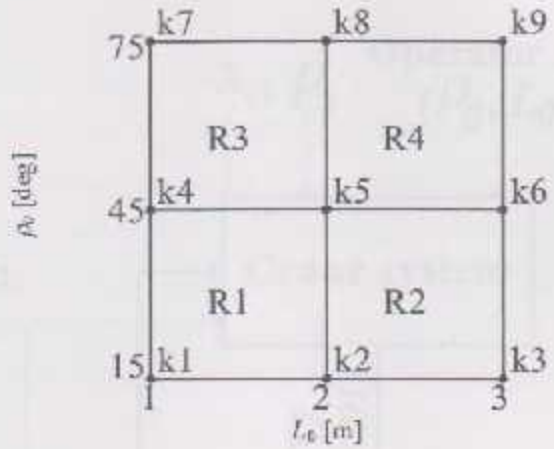

Figure (4.5.a): operating regions R(i), i =1…4

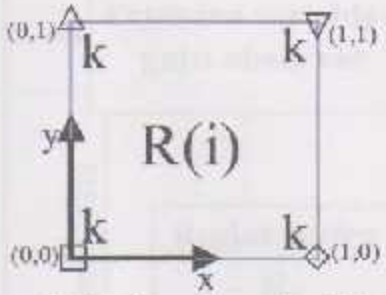

Figure (4.5.b): Operating region R(i) with gains on the corners □, ◊, Δ, and ∇

In figure (4.5.b) every corner is denoted by symbol, where □ denotes the lower left corner, ◊ denotes the lower right corner, Δ denotes the upper left corner, and ∇ denotes the upper right corner. While x & y denotes the local coordinates for the region i, the need for these symbols and local coordinates will appear in the interpolation of the gains inside every region later in this chapter.

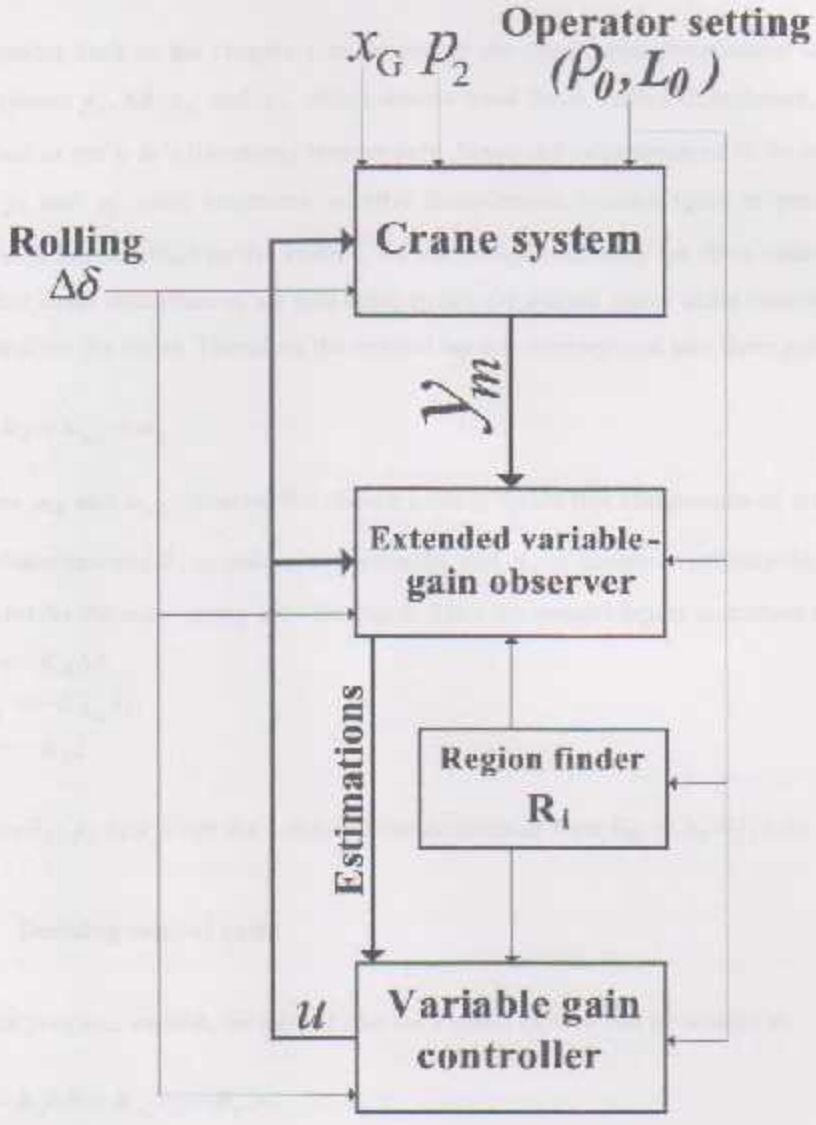

Figure (4.6): Block diagram of a control system

4.5 Controller design

Returning back to the chapter 1 to remember the considered disturbances acting on the system p_z, $\Delta\delta$, x_G and y_G which denote wind force, rolling disturbance, and the motion in the x & y directions respectively. Since $\Delta\delta$ was assumed to be measured and p_z and x_G were estimated, y_G after linearization became equal to zero, which means it has no effect on the system, we can compensate only for these disturbances. Beside those disturbances we will compensate for system states using state feedback control for the crane. Therefore the control input u decomposed into three parts,

$$u = u_{\delta} + u_{x_G} + u_z \tag{4.17}$$

where u_{δ} and u_{x_G}, denotes the chosen control inputs that compensate or act against the disturbances $\Delta\delta$, x_G and p_z respectively, and u_z is chosen to provide the optimal control for the crane using state feedback. Then the control inputs expressed as

$$\begin{aligned} u_{\delta} &= -K_{\delta}\Delta\delta \\ u_{x_G} &= -K_{x_G}\hat{x}_G \\ u_z &= -K_z\hat{z} \end{aligned} \tag{4.18}$$

where $\hat{x}_G$, $\hat{p}_z$ and $\hat{z}$ are the estimated states obtained from Eq. (4.6, 4.7, 4.8).

4.6 Defining control gains

In the previous section, we agreed that the control input u can be written as

$$u = -K_{\delta}\Delta\delta - K_{x_G}\hat{x}_G - K_z\hat{z} \tag{4.19}$$

Substituting Eq. (4.19) value in Eq. (3.9), yields

$$\dot{z} = (A - BK_z)z + (E - BK_{\delta})\Delta\delta + (F - BK_{x_G})x_G \tag{4.20}$$

so as a first thought to find the value of disturbances gains that makes the terms which include the disturbances to vanish or become zero, as follow

$$E - BK_{\delta} = 0$$

$$F - BK_{x_0} = 0 \tag{4.21}$$

This solution can performed using algebraic techniques to avoid the inverse of non square matrix B, any way this method will not give a satisfying result, so another solution must be performed.

The method that we will perform depends on the act of control inputs mentioned in chapter one $\Delta\rho$, ΔL, and ΔD. When disturbance act on the system how should these control inputs act or work in order to keep the position of the payload steady ($\Delta x_2 = 0$ and $\Delta y_2 = 0$), this is done using partial derivation, as we will see next.

4.6.1 Defining K_{δ}

The rolling motion of the ship affects the payload through the structure of the crane; this tends to disturb the equilibrium position of the payload as demonstrated in Fig. (4.7) It is clear from this figure, that a small roll angle $\Delta\delta$ produces a large shift in the equilibrium position of the payload which induces the unwanted pendulation. The idea behind static disturbance compensation is to find an input vector proportional to the rolling disturbance that can maintain the position of the payload in place as much as possible. This can be achieved in three steps as shown in Figs. (4.8-4.10). In the first step, the luff angle $\Delta\rho$ is employed to prevent the boom from changing its orientation with respect to the horizontal reference by maintaining $\beta = \beta_0$. In the second step the coordinate of the payload is recovered by displacing the position of the lower suspension point through ΔD. In the third step the error in the y-coordinate

is eliminated by changing the length of the upper cable through ΔL, these three step have to be executed in parallel (at the same time). To find the numerical values of the corresponding three inputs, set the changes in x_2 and y_2 resulting from rolling to be zero, i.e.,

$$\Delta x_{20} \approx \frac{\partial x_{20}}{\partial \delta}\Delta\delta + \frac{\partial x_{20}}{\partial \beta}\Delta\beta + \frac{\partial x_{20}}{\partial L}\Delta L + \frac{\partial x_{20}}{\partial D}\Delta D + \frac{\partial x_{20}}{\partial x_G}\Delta x_G = 0$$

$$\Delta y_{20} \approx \frac{\partial y_{20}}{\partial \delta}\Delta\delta + \frac{\partial y_{20}}{\partial \beta}\Delta\beta + \frac{\partial y_{20}}{\partial L}\Delta L + \frac{\partial y_{20}}{\partial D}\Delta D + \frac{\partial y_{20}}{\partial x_G}\Delta x_G = 0 \qquad (4.22)$$

The condition $\beta = \beta_0$ can be fulfilled by setting $\Delta\beta = 0$, and achieved by setting $\Delta\rho = -\Delta\delta$, and then the Eq. (4.22) can be written in the matrix form as

$$\underbrace{\begin{bmatrix} 1 & 0 & 0 \\ 0 & \partial x_2/\partial L & \partial x_2/\partial D \\ 0 & \partial y_2/\partial L & \partial x_2/\partial D \end{bmatrix}}_{A_\delta} \underbrace{\begin{bmatrix} \Delta\rho \\ \Delta L \\ \Delta D \end{bmatrix}}_{\Lambda_\delta} = \underbrace{\begin{bmatrix} 1 \\ \partial x_2/\partial\delta \\ \partial y_2/\partial\delta \end{bmatrix}}_{B_\delta} \qquad (4.23)$$

Then

$$K_\delta = A_\delta^{-1} B_\delta \qquad (4.24)$$

Simulation results for controlled and uncontrolled system under the effect of $\Delta\delta$ with amplitude 3° and frequency close to the first natural frequency of the system are shown in Fig. (4.11), in this figure we see the two responses of the two systems.

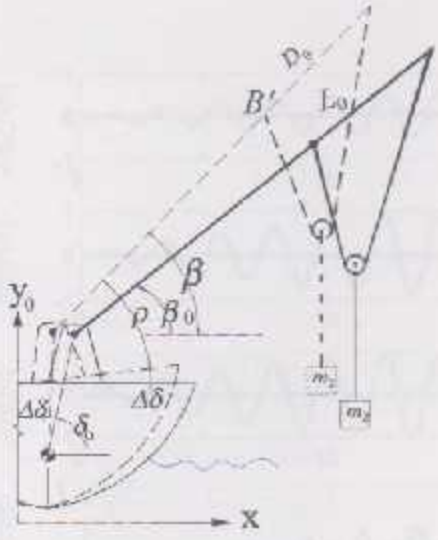

Figure 4.7: Rolling through $\Delta\delta$

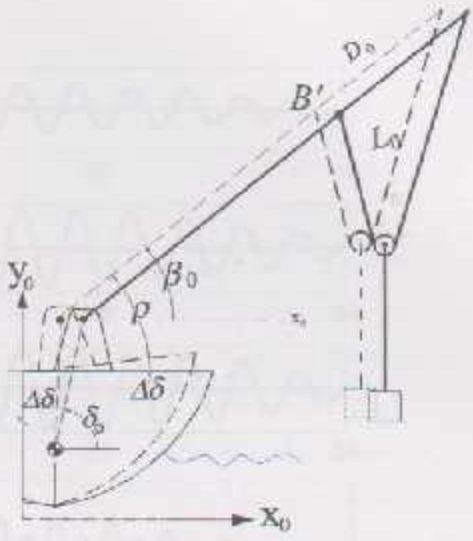

Figure 4.8: Compensation through $\Delta\rho$

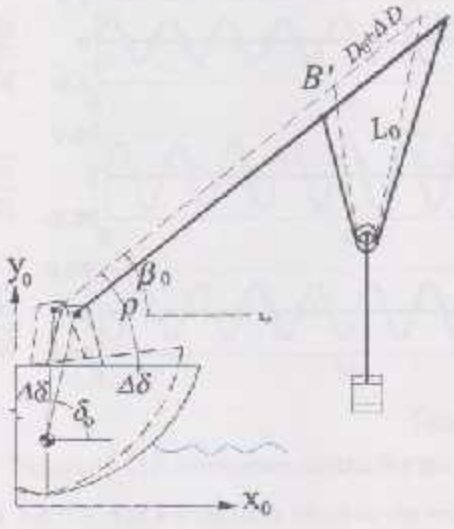

Figure 4.9: Compensation through ΔD

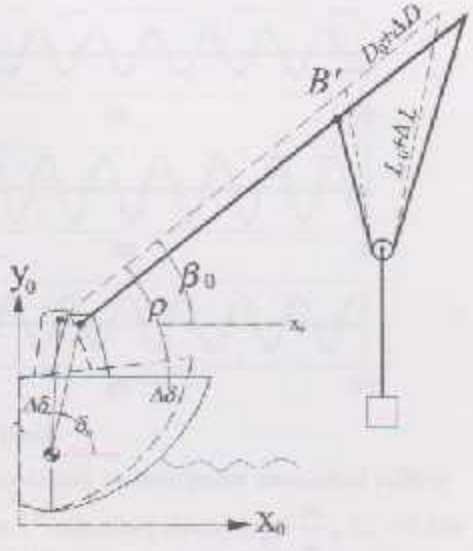

Figure 4.10: Compensation through ΔL

——Original position ------Current position

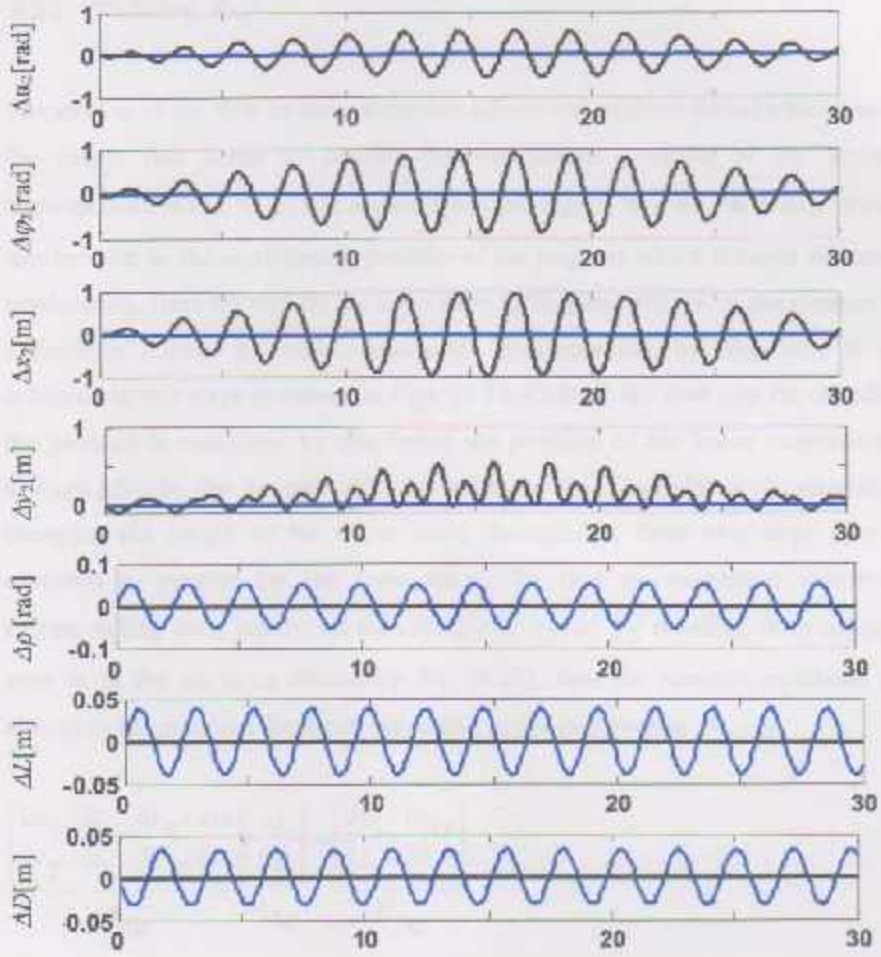

Figure (4.11): simulation results for the linearized system under sinusoidal rolling ($\Delta\delta = 3^{\circ}$) at a frequency close to the crane 1st eigenfrequency, $\rho_0 = -\frac{\pi}{4}$, $L_0 = -1.5\,m$

_____ controlled _____ uncontrolled

4.6.2 Defining Kx_G

The motion of the ship in the x-direction affects the payload through the structure of the crane; this tends to disturb the equilibrium position of the payload as demonstrated in Fig. (4.12). It is clear from this figure, that any shift Δx_G produces a similar shift in the equilibrium position of the payload which induces the unwanted pendulation. Here we will do the same as in rolling disturbance to compensate for the x-direction motion by static disturbance compensation, but this time it can be achieved in two steps as shown in Figs. (4.13-4.14). In the first step the coordinate of the payload is recovered by displacing the position of the lower suspension point through ΔD. In the second step the error in the y-coordinate is eliminated by changing the length of the upper cable through ΔL, these two steps have to be executed in parallel (at the same time). To find the numerical values of the corresponding three inputs, set the changes in x_2 and y_2 resulting from rolling to be zero as in the previous subsection Eq. (4.22), then the resulted equations can be written in the matrices form corresponding to the disturbance Δx_G as,

$$\underbrace{\begin{bmatrix} \partial x_2/\partial L & \partial x_2/\partial D \\ \partial y_2/\partial L & \partial y_2/\partial D \end{bmatrix}}_{A_{x_G}} \underbrace{\begin{bmatrix} \Delta L \\ \Delta D \end{bmatrix}}_{u_{x_G}} = \underbrace{\begin{bmatrix} \partial x_2/\partial x_G \\ \partial y_2/\partial x_G \end{bmatrix}}_{B_{x_G}} \tag{4.25}$$

Then,

$$K_{x_G} = \begin{bmatrix} 0 \\ A_{x_G}^{-1} B_{x_G} \end{bmatrix} \tag{4.26}$$

Simulation results for controlled and uncontrolled system under the effect of Δx_G with amplitude 10 *cm* and frequency close to the natural frequency of the system shown in Fig. (4.15)

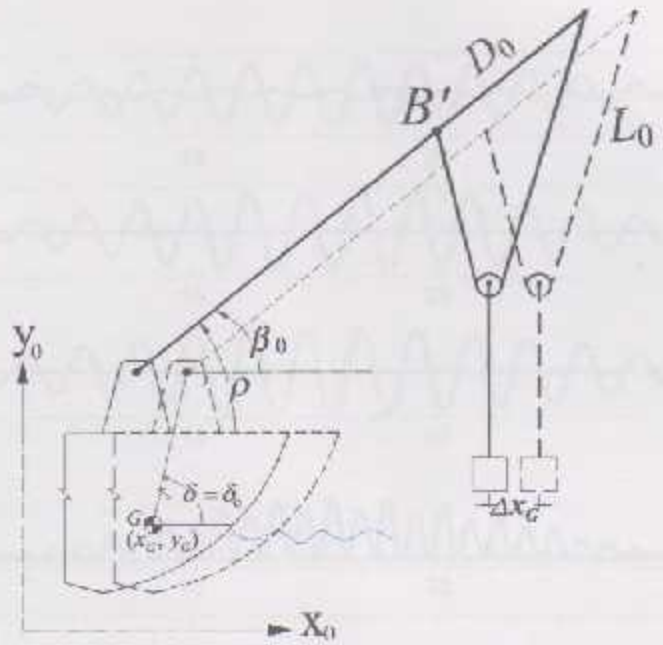

Figure(4.12): x_G effect on the crane system

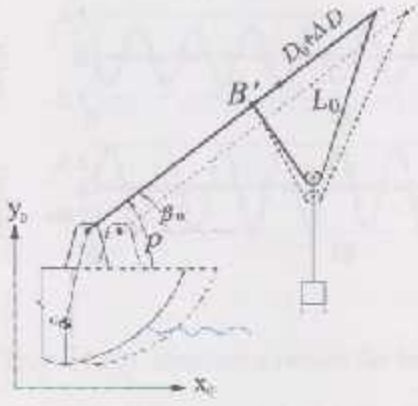

Figure(4.13): Compensation through ΔD

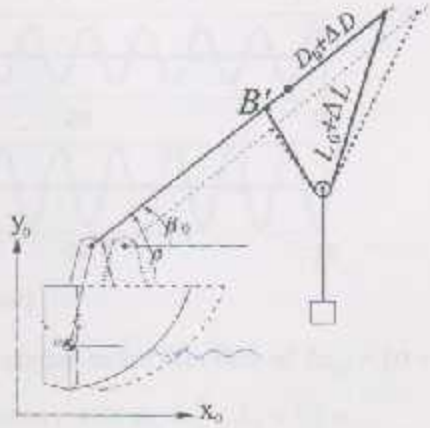

Figure(4.14): Compensation through ΔL

------ Original position

—— Current position

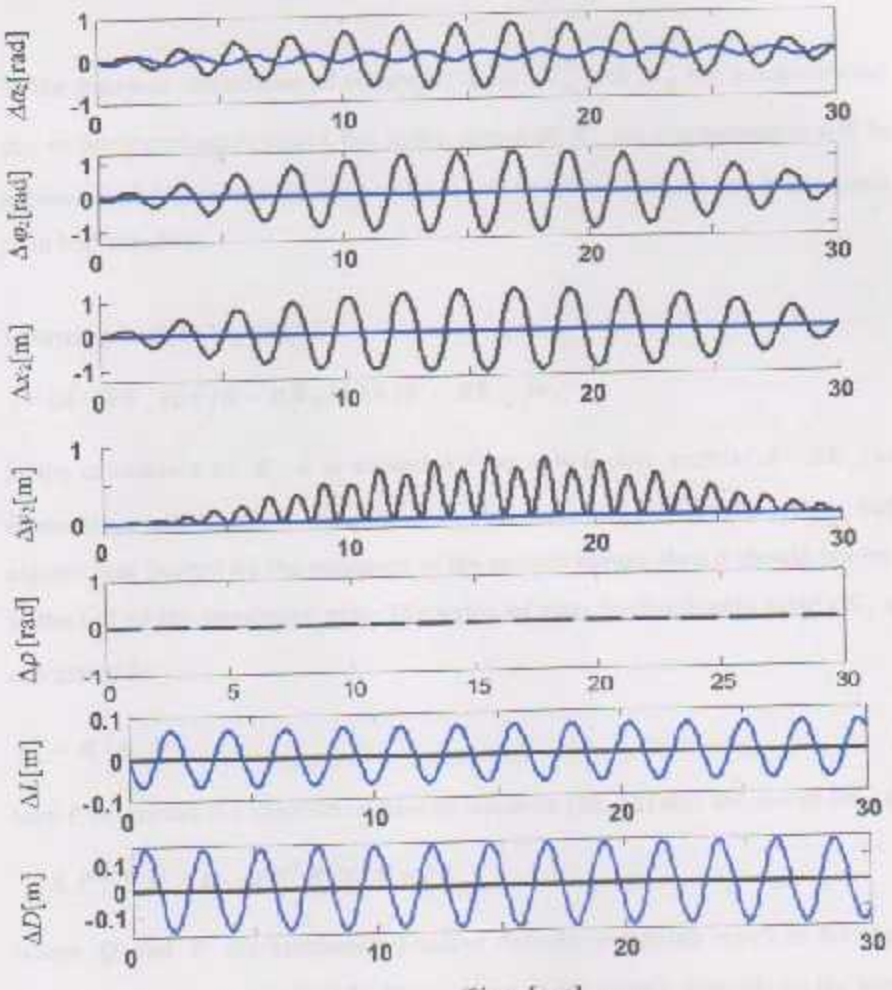

Figure (4.15): simulation results for linearized system under the effect of $\Delta x_G = 10\ cm$, and frequency close to the eigenfrequency with $\rho_0 = \frac{\pi}{4}$, $L_0 = 1.5\,m$

_____ controlled _____uncontrolled

4.6.3 Defining K_z

In the previous definitions of controller gains K_{x_c} and K_δ the compensation were due to the disturbances effect, but in the design of K_z the compensation will be for a nonzero initial condition that expected to act on the system, or due to the wind force p_2 in bad weathers.

Returning back to Eq. (4.20),

$$\dot{z} = (A - BK_z)z + (E - BK_\delta)\Delta\delta + (F - BK_{x_c})x_G$$

In the calculation of K_z it is wanted for the new system matrix $(A - BK_z)$ to have eigenvalues with negative real part to provide more stability for the system, but these eigenvalues limited by the actuators of the control inputs, then it should not be so far to the left of the imaginary axis. The value of state feedback gain matrix K_z can be calculated as,

$$K_z = R^{-1}B^T P \tag{4.27}$$

here P represents the solution of Riccati equation [20, 11] that we saw in Eq. (4.15)

$$A_z P + P A_z^T + Q_z - P C_z^T R_z^{-1} C_z P = 0$$

where Q and R are symmetric positive definite weighting matrices for the states and the inputs respectively [17]. Eigenvalues of the system depends on the numerical structure of these matrices, and then the crane system will perform the required behavior of the dynamic response. Since we use the value of the estimated states from the PI-Observer it is necessary to the observer to be faster that the real system, this is achieved by placing the eigenvalues of the observer farther to the left of the eigenvalues of the control system of the crane model by making the required tuning to the structure of Q and R matrices.

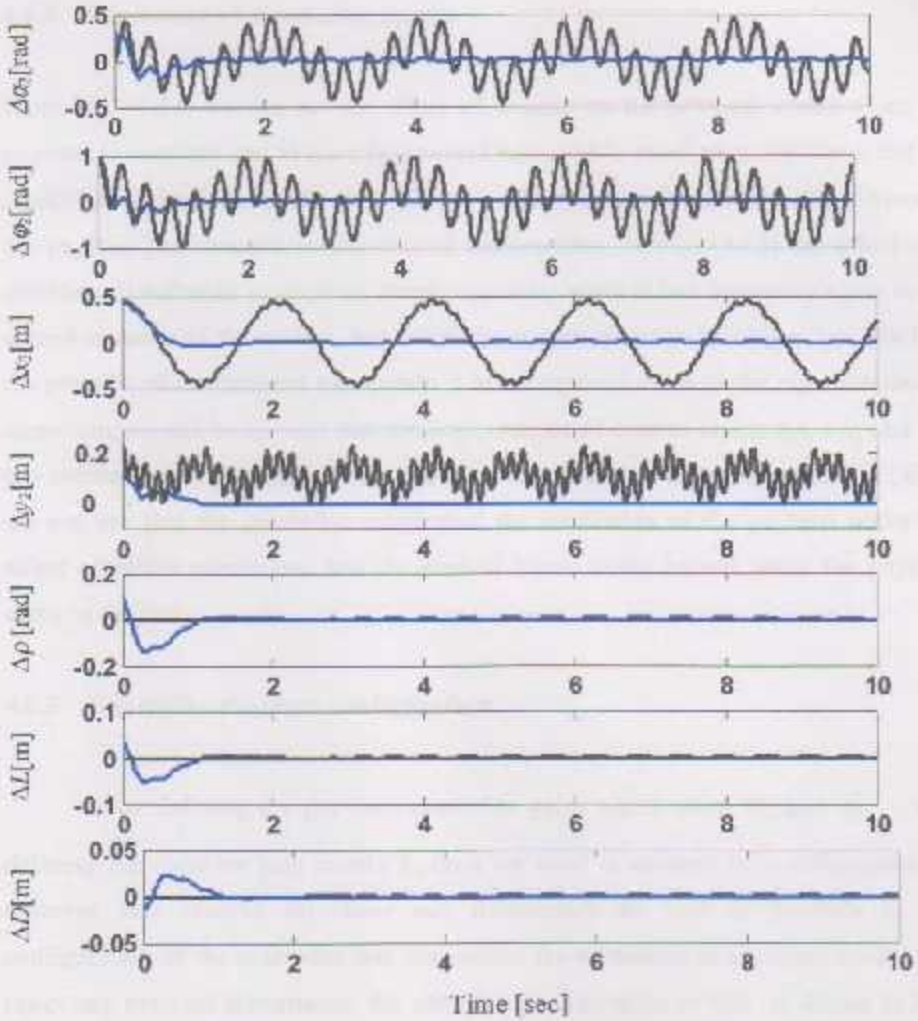

Figure (4.16): simulation results for linearized system under the effect of initial condition $\phi_2(0) = 1\ rad$, and frequency close to the eigenfrequency with $\rho_0 = \frac{\pi}{4}$, $L_0 = 1.5m$

____ controlled _____uncontrolled

4.6.4 Discussion of simulation results

From Fig. (4.11) we can see the effect of rolling on the payload, which make the payload to resonate and to have large amplitude within small ranges of time, but the controlled system has nearly no oscillation which means that the controller brought the payload performance to the desired performance. In Fig. (4.15) the effect of x direction disturbance x_G appears clearly specially when it has frequency close to the eigenfrequency of the system, but when the system is controlled it has no effect on the position of the payload even when it has frequency close to the eigenfrequency, something should be noticed that the performance of control inputs $\Delta\rho$, ΔL, and ΔD is a continuous performance since this disturbance is continuous. Also in Fig. (4.16) we can see that the controller suppressed the oscillation of the payload under the effect of initial conditions, and the control inputs come to rest when the payload come to the rest.

4.6.5 Controller observer configuration

After defining the previous controller gains which were, K_s and K_{x_G}, and defining the observer gain matrix L_e then we need to connect the configuration of observer that observe all states and disturbance as well as possible to the configuration of the controller that can reduce the vibrations in the crane model and reject any external disturbance, the simulink configuration of this is shown in Fig. (4.17). From this simulink structure we can see the real system controlled by state feedback control, in addition the same controller can be used to cancel the effects of the unknown disturbances p_2 and x_G which can be estimated by using this configuration. The error signal is the difference between the output of real system and that of the observer.

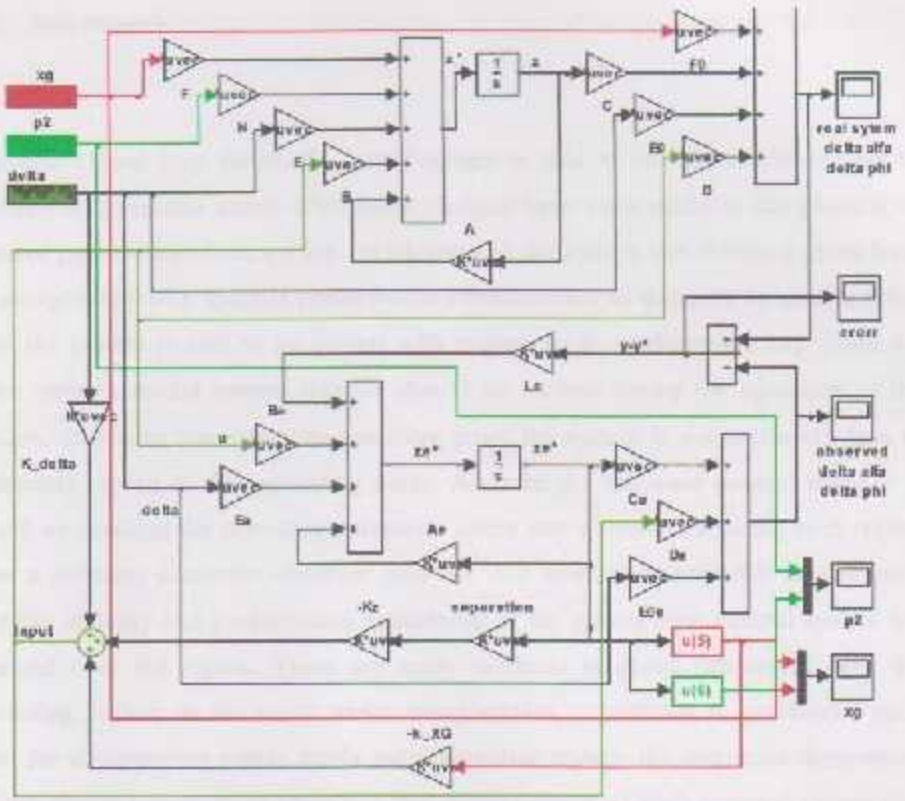

Figure (4.17): simulink structure of the controller observer configuration of linear system

4.7 Robustness

A stable closed loop feedback control system is said to be robust with respect to stability if it remains stable after some changes have been made in the physical or control parameters of the system. In addition, if the system still fulfills a given level of acceptability of a specific performance criterion such as damping or settling time, then the system is said to be robust with respect to its performance [5]. Since we have variable model system stability should be studied during the operation of the system, so not to come into an operating point the system is not stable or close to instability region at this operating point. Accordingly, the used control strategy is based on dividing the operating parameter space into 4 uniform regions; each region uses a different controller-observer gain set. The size of the region is limited such that the stability and performance robustness of the closed loop control system are ensured over the region. There are many methods to check robustness over the operating region; in the crane under consideration, robustness is guaranteed such that, for all operating points inside each individual region, the dominant eigenvalues of the closed loop system remain in the neighborhood of their nominal values that correspond to the calculated gain of the controller.

But at which point inside each region the gain should be calculated, to do so we will consider the region R4 shown in Fig. (4.5.a & 4.5.b), and as first trial we will consider that the region is covered by a constant gain controller and a constant gain observer, and assume that the gain matrix is calculated at the center of the region, i.e., the observer gain matrix and the controller gain matrix are calculated at $\rho_0 = (45°+75°)/2 = 60°$ and $L_0 = (L_{02}+L_{03})/2 = 2.5$m. The weighting matrices $\boldsymbol{Q}$ and $\boldsymbol{R}$ are selected such that, sufficient damping is created in the crane with adequate relative stability for the actuators constraint $|u| \leq \max(u)$. The current eigenvalues of the closed loop system are obtained by solving the polynomial $|\lambda I - \boldsymbol{A} + \boldsymbol{B}\boldsymbol{K}_r| = 0$. Since

A and B vary with the current operating point (L_0, ρ_0) inside the current region, the eigenvalues also vary consequently.

The locus of the two dominant eigenvalues (λ_1 and λ_2) due to the variation in L_0 and ρ_0 are shown in Fig. (4.18); the nominal values (design values) of the dominant eigenvalues are denoted by black bold * and the values at the lower left and lower right corners of the region are denoted by □ and ◊ respectively, and the values at the upper left and upper right corners are denoted by Δ and ∇ respectively. The shaded blue regions represent the locus of the dominant eigenvalues for all possible values of ρ_0 and L_0 inside R4. It can be easily recognized that as the operating point moves toward the lower right corner of the region (L_0 increases and ρ_0 decreases), the eigenvalue λ_1 become closer to its imaginary axis, which means that the crane may lose a considerable percentage of its relative stability with a reduction in the damping ratio.

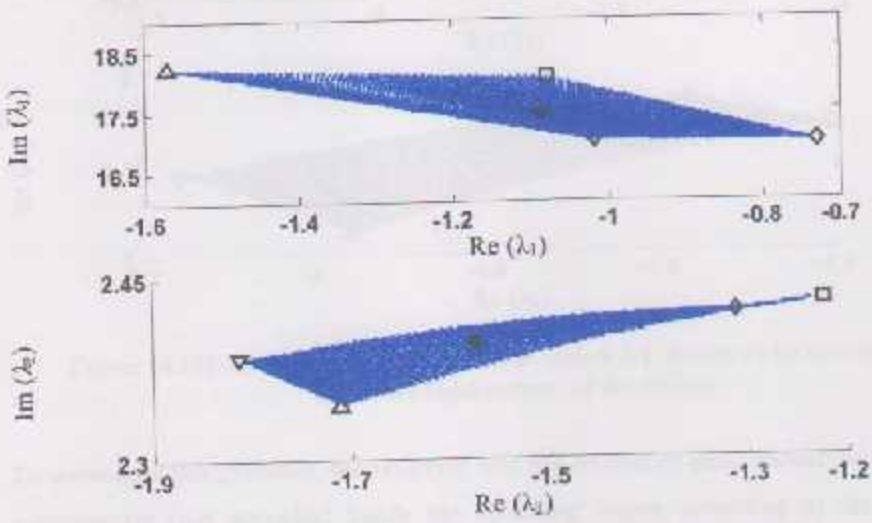

Figure (4.18): root locus for system in the region R4, design point considered at the center of the region

This result lead to change the design point inside R4 to be the lower right corner, since the poles at this point comes too close to the imaginary axis. In this case, the locus of the dominant eigenvalues are shown in Fig. (4.19). It can be seen that for all possible operating points inside R4, all the eigenvalues of λ_1 lay to the left of its nominal value; this of course improves the corresponding relative stability and damping ratio. But, in the region of λ_2 we notice that the lower right operating point moves to the left of its nominal value, this eigenvalue some of its relative stability with a considerable reduction in the damping ratio. Therefore, neither the center point nor the lower right corner of the region can give a satisfactory selection of the design point.

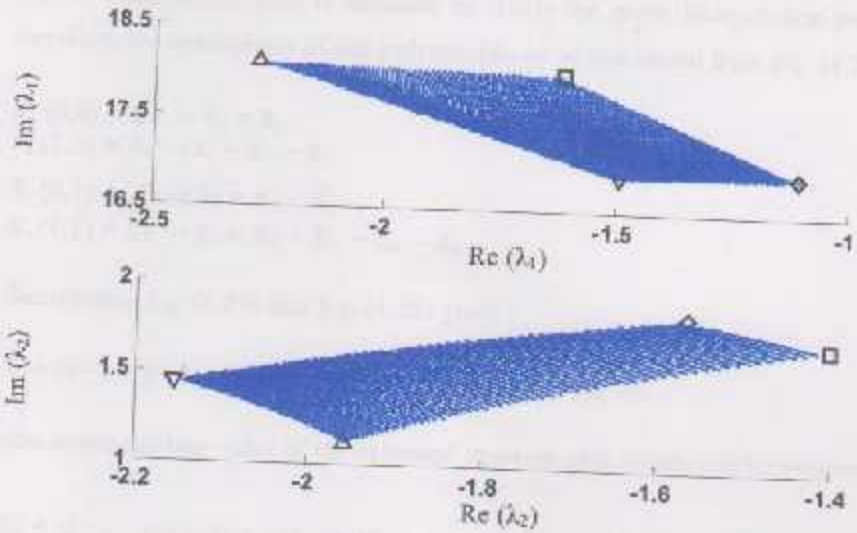

Figure (4.19): root locus for system in the region R4, design point considered at the lower right corner of the region

To overcome this problem, the observer and the controller gains should be updated continuously (not stepwise) inside the operating region according to the current (instantaneous) value of the pair L_0 and ρ_0 to preserve the damping ratio and relative stability over the region. In this way, the gains are calculated at each individual

corner of the considered region; the weight matrices are chosen to produce nearly the same relative stability and damping at each corner, and each corner gain should provide a stable operation of the crane for all possible operating points inside the region. The total value of the controller gain, corresponding to the current operating point, is described by the 2-D interpolation polynomial

$$K_c = K_c(x,y) = k_1 + k_2 x + k_3 y + k_4 xy \tag{4.28}$$

where x and y denote the local coordinate axes of the region as shown in Fig. (4.5.b), and $k_1,\ldots,k_4$ denote the polynomial coefficient matrices, the numerical values of the these coefficient matrices depend on the gains associated with the corners of the region. Each corner gain is assumed to satisfy the given interpolation polynomial; therefore, the coefficients of this polynomial can be calculated from Eq. (4.28) to get

$$\begin{aligned}
&K_c(0,0) = K_{\square} \rightarrow k_1 = K_{\square} \\
&K_c(1,0) = K_{\circ} \rightarrow k_2 = K_{\circ} - K_{\square} \\
&K_c(0,1) = K_{\triangle} \rightarrow k_3 = K_{\triangle} - K_{\square} \\
&K_c(1,1) = K_{\triangledown} \rightarrow k_4 = K_{\triangledown} + K_{\square} - K_{\circ} - K_{\triangle}.
\end{aligned} \tag{4.29}$$

Substituting Eq. (4.29) into Eq. (4.28) gives

$$K_c = (1-x-y+xy)K_{\square} + (x-xy)K_{\circ} + (y-xy)K_{\triangle} + (xy)K_{\triangledown} \tag{4.30}$$

also corresponding value of the extended observer gain matrix can be expressed as

$$L_e = (1-x-y+xy)L_{\square} + (x-xy)L_{\circ} + (y-xy)L_{\triangle} + (xy)L_{\triangledown} \tag{4.31}$$

and the rolling disturbance compensator gain matrix is described by

$$K_\delta = (1-x-y+xy)K_{\delta\square} + (x-xy)K_{\delta\circ} + (y-xy)K_{\delta\triangle} + (xy)K_{\delta\triangledown} \tag{4.32}$$

finally the x-direction disturbance compensator gain matrix is described by

$$Kx_G = (1-x-y+xy)Kx_{G\square} + (x-xy)Kx_{G\circ} + (y-xy)Kx_{G\triangle} + (xy)Kx_{G\triangledown} \tag{4.33}$$

This includes that the gains can be updated continuously according to the local x- and y-coordinates of the current operating point. The locus of the dominant eigenvalues corresponding to R4 is shown in Fig. (4.20). Note that the blue regions of the dominant eigenvalues are considerably contracted. Therefore, the relative stability and the damping property are preserved for all operating points inside the region. Another significant advantage acquired using this interpolation method is that, the problem which may appear due to a stepwise change of the controller gain between two different regions is avoided.

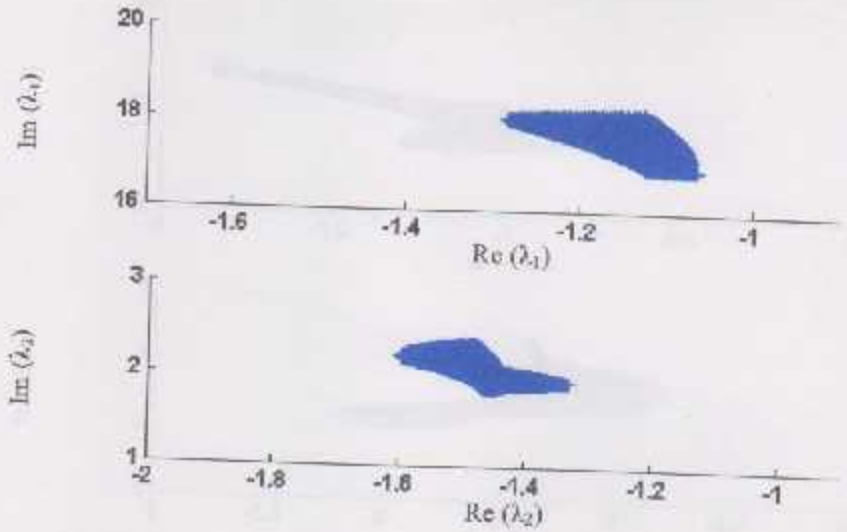

Figure (4.20): root locus for system in the region R_4 using continuous gain method

Now we want to apply interpolation to all regions $R_1;\ldots;R_4$. Fig. (4.21) show the locus of the dominant eigenvalues based on the continuous gain method for all admissible equilibrium points inside the entire working space of the crane. i.e., for the control law covering the 4 operating regions. It can be recognized that stability

and damping properties are fulfilled. The previous plots are based on the nominal value of the payload mass, i.e., m_{20} = 5kg.In practice, the payload mass is uncertain; it depends on the cargo being hoisted and may vary within a known interval. Therefore, the crane must be also robust varying values of the payload. In Figs.(4.22) and 4.23 the regions of the dominant eigenvalues are plotted for entire working space of the crane for tow different payload mass $m_2 \in [0.5;1.5]m_{20}$. Note that the stability is fulfilled for all parameters under consideration.

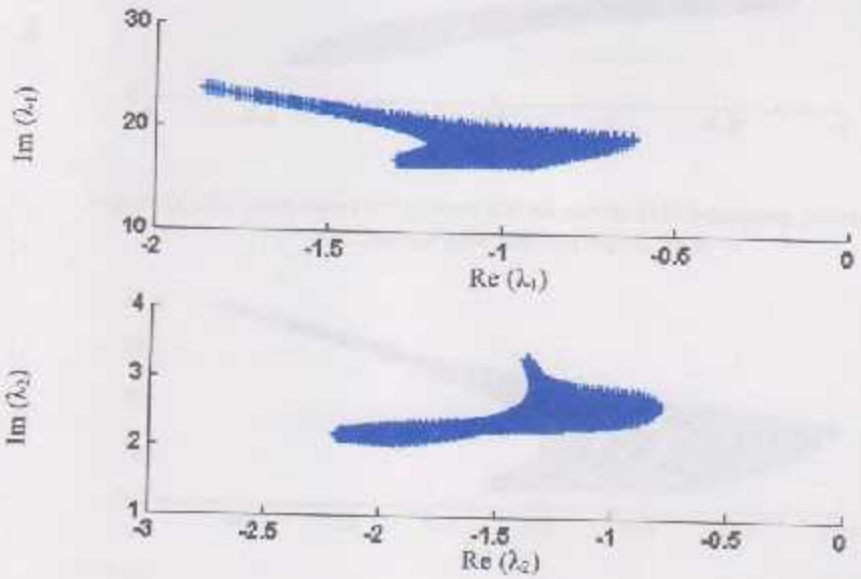

Figure (4.21): root locus for system for all admissible operating points using continuous gain method , m_{20}=5kg

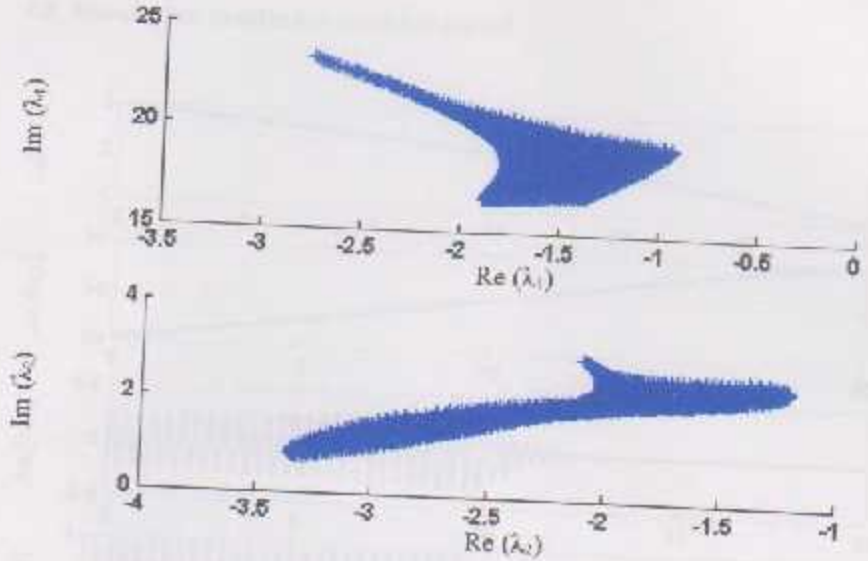

Figure (4.22): root locus for system for all admissible operating points using continuous gain method $m_2=1.5m_{20}$

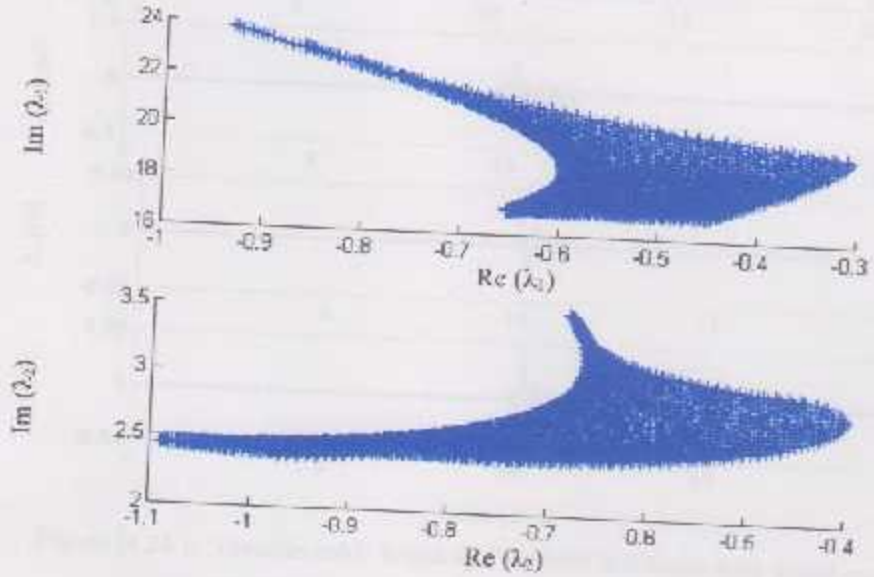

Figure (4.23): root locus for system for all admissible operating points using continuous gain method $m_2=0.5m_{20}$

4.8 Simulation results for variable model

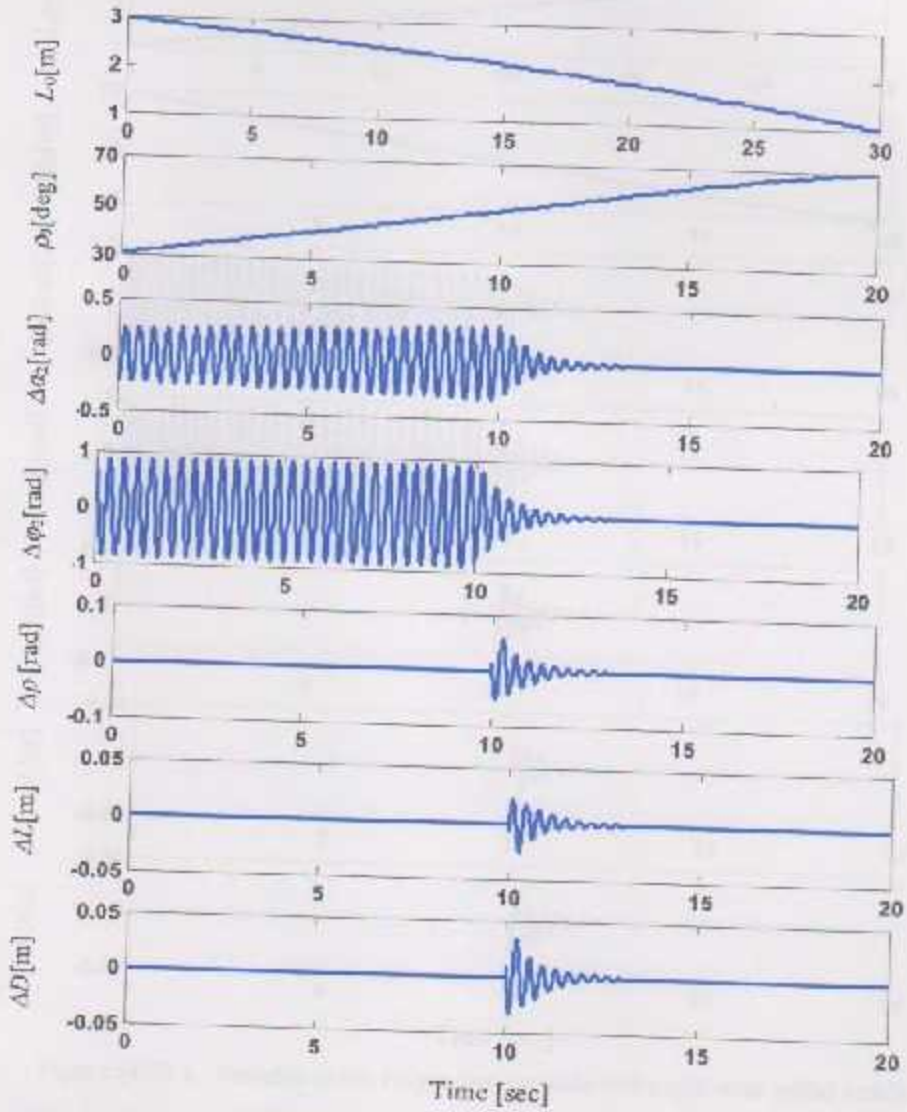

Figure (4.24): Variable cable length and variable luff angle with initial condition $\phi_2(0) = 1$ rad, controller is turned on after 10 sec.

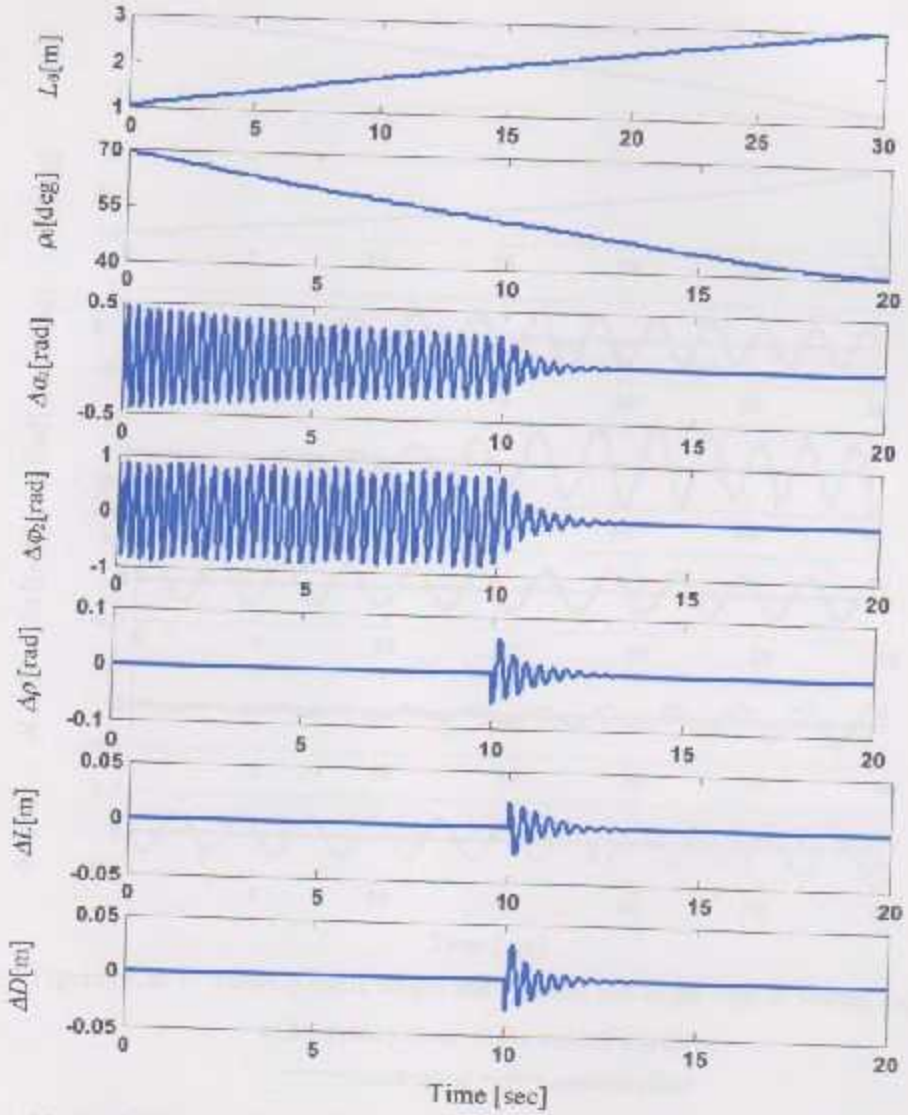

Figure (4.25): Variable cable length and variable luff angle with initial condition $\phi_2(0) = 1$ rad, controller is turned on after 10 sec.

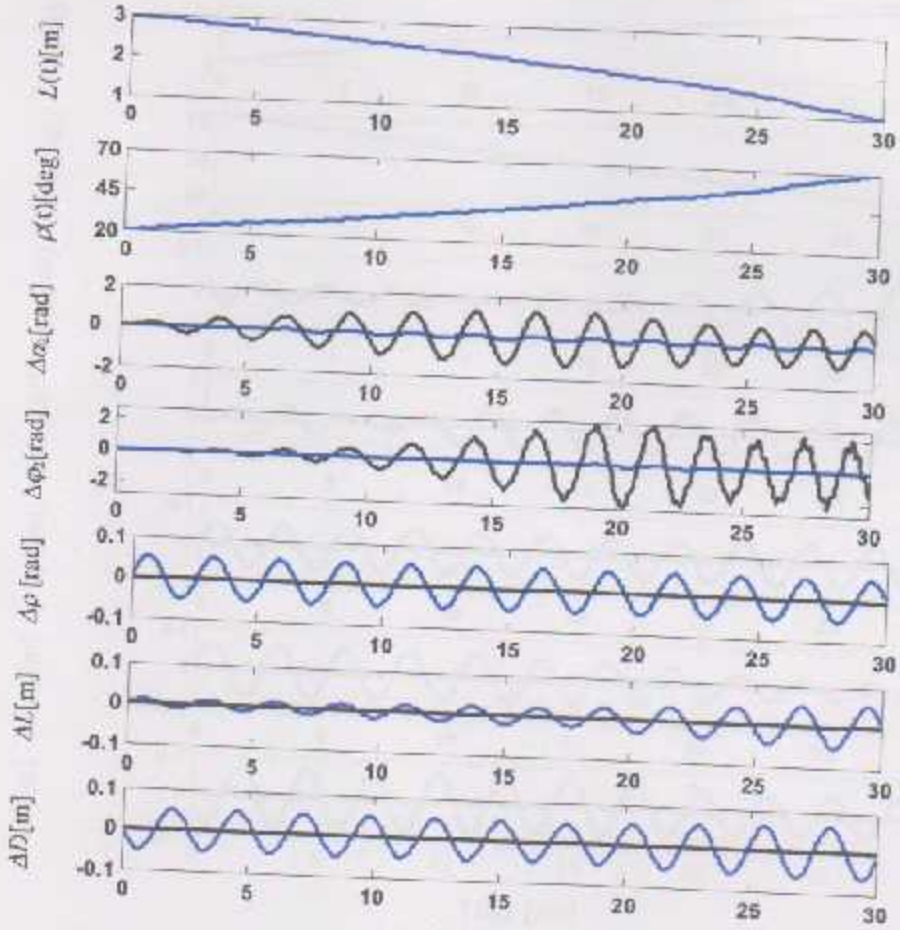

Figure (4.26): Variable cable length and variable luff angle with 3° rolling angle of frequency close to the eigenfrequency

—— controlled —— uncontrolled

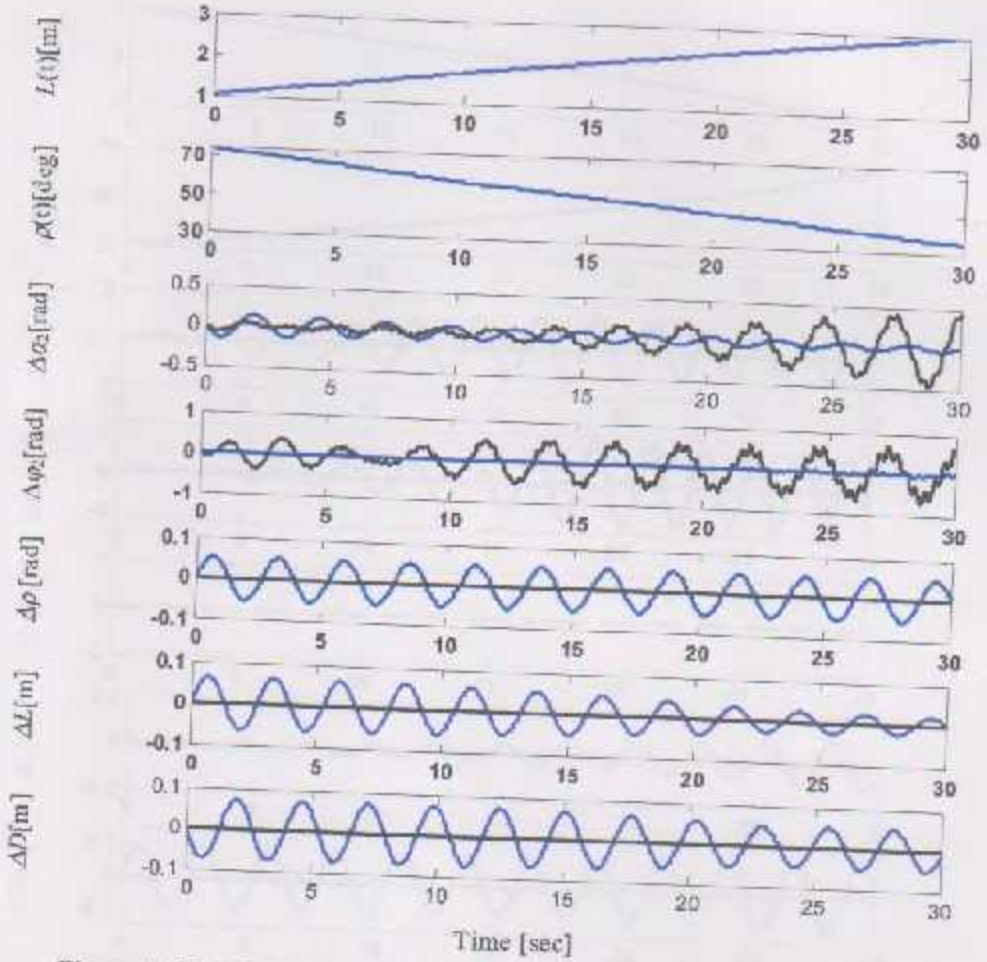

Figure (4.27): Variable cable length and variable luff angle with 3° rolling angle of frequency close to the eigenfrequency

controlled —— uncontrolled

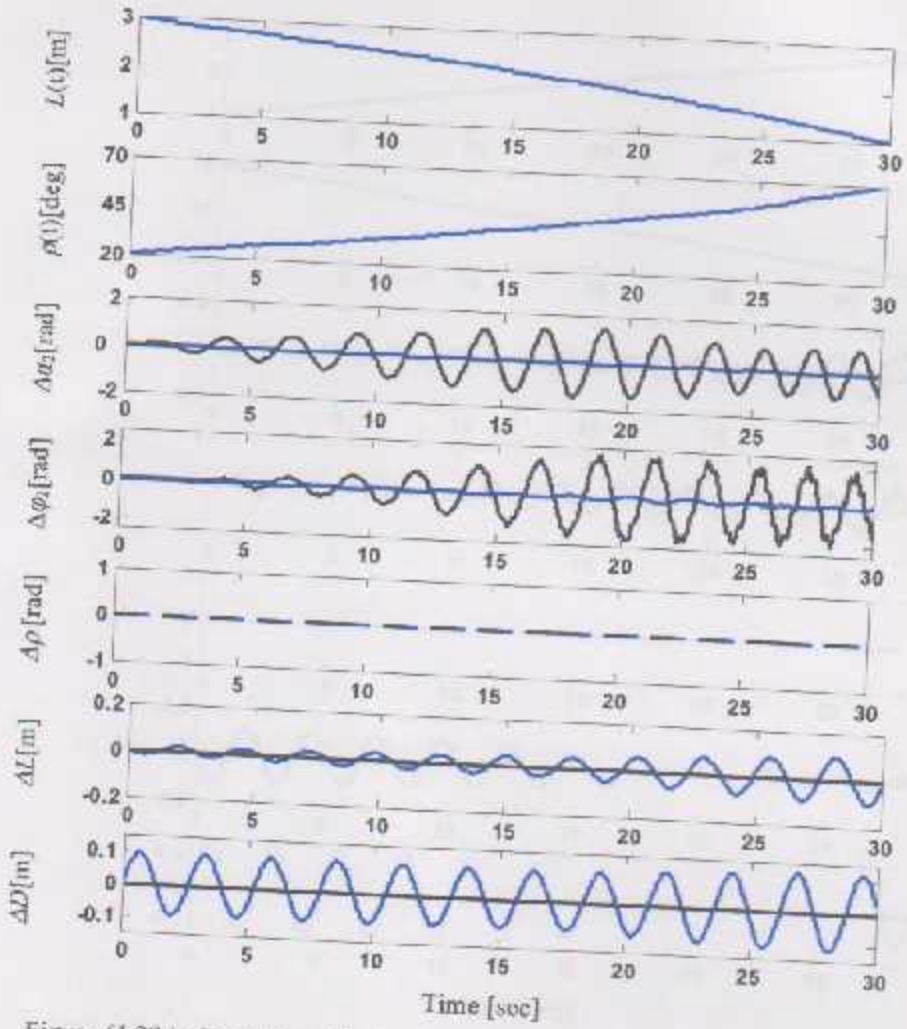

Figure (4.28): Variable cable length and variable luff angle with 5 cm sinusoidal disturbance in the x-direction of frequency close to the eigenfrequency

controlled —— uncontrolled

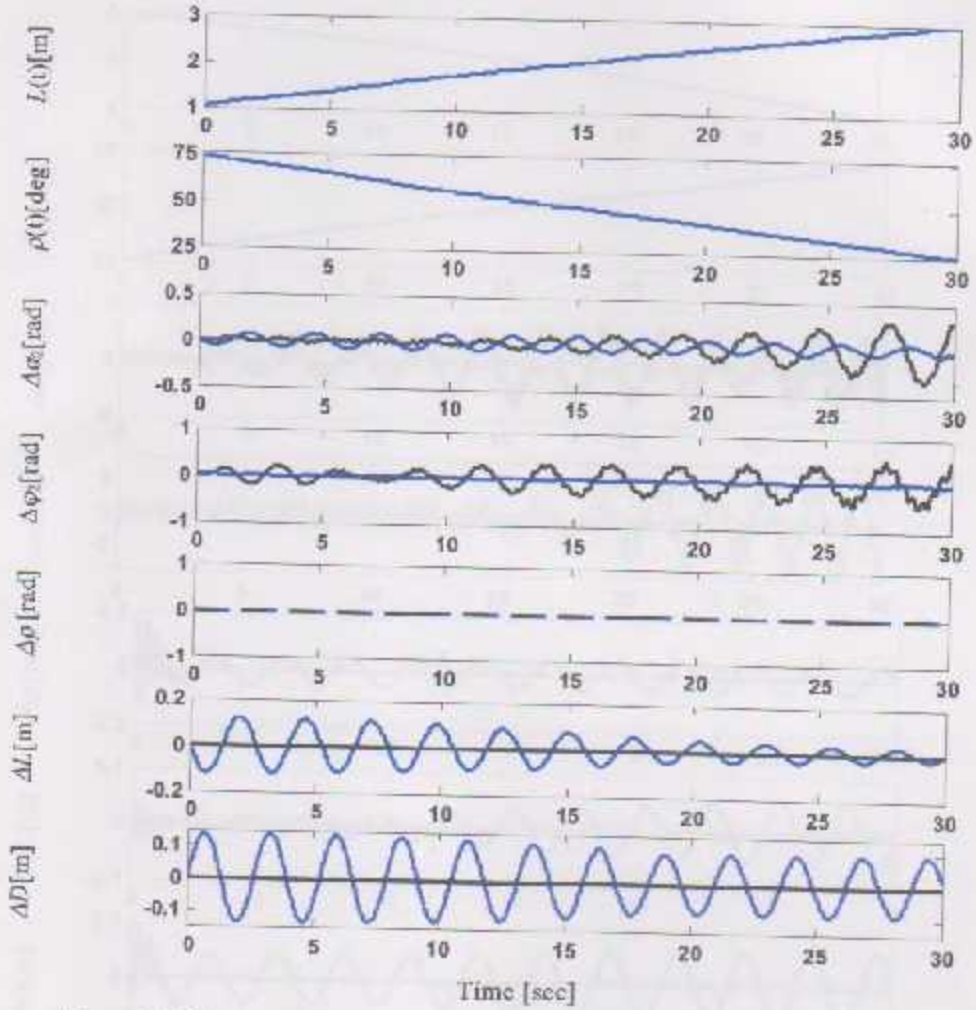

Figure (4.29): Variable cable length and variable luff angle with 5 cm sinusoidal disturbance in the x-direction of frequency close to the eigenfrequency

——— controlled —— uncontrolled

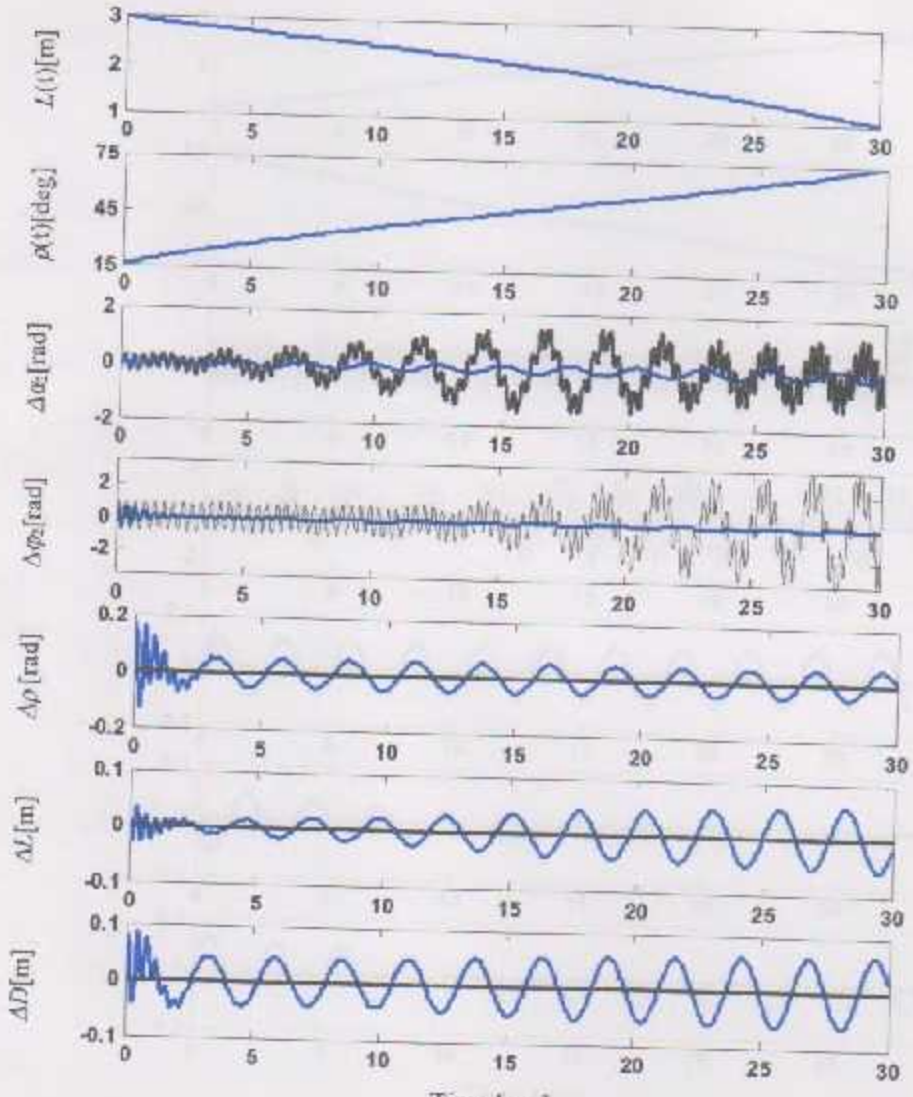

Figure (4.30): Variable cable length and variable luff angle with $\phi_2(0) = 1$ rad, 5 cm sinusoidal disturbance in the x-direction, and 3° sinusoidal rolling angle of frequency close to the eigenfrequency —— controlled —— uncontrolled

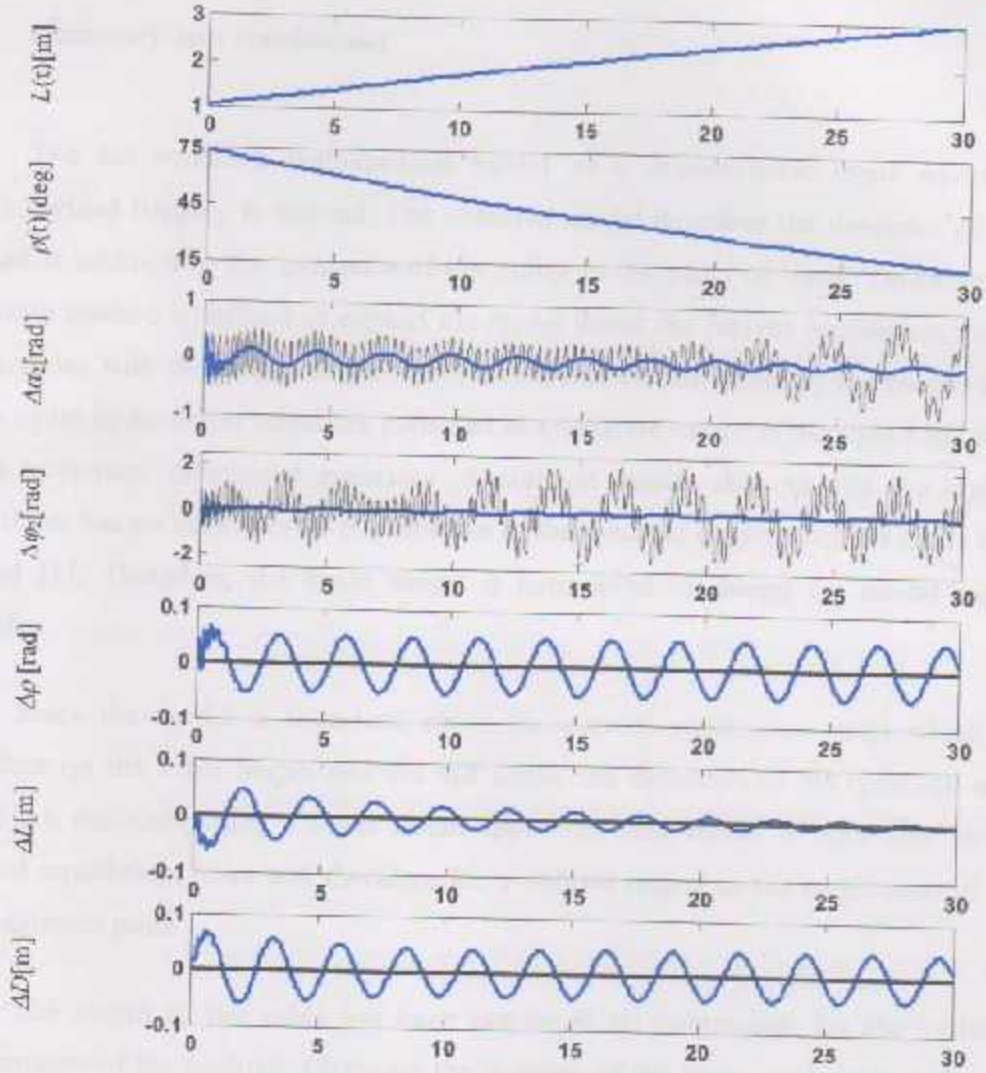

Figure (4.31): Variable cable length and variable luff angle with $\phi_2(0) = 1$ rad, 5 cm sinusoidal disturbance in the x-direction, and 3° sinusoidal rolling angle of frequency close to the eigenfrequency —— controlled —— uncontrolled

Chapter five

Summary, conclusions and recommendations

5.1 Summary and conclusions

The full nonlinear mathematical model of a ship-mounted crane equipped with Maryland Rigging is derived. The obtained model describes the dynamics of the payload in addition to the dynamics of the pulley in the plane of them. Taylor series expansion method is utilized to expand the model about the current equilibrium point, which varies with the length of the upper cable and the luff angle of the boom. The higher order or nonlinear terms are collected in a separate vector in the right hand side of the governing differential equations. Simulation results showed that the higher order terms has no considerable contribution in the dynamic response of the crane and payload [1]. Therefore, the linear model is considered to design the model-based controller.

Since the model is linearized about the current equilibrium point which is dependent on the cable length and the luff angle, the dynamics of the (payload and pulley) are described using a multi model approach; each model is valid only for a specified equilibrium point and therefore for a defined region in the neighborhood of the equilibrium point.

The length of the cable has been employed to compensate for the vertical displacements of the payload. Changing the position of the lower suspension point of the upper cable gave a significant effect in controlling the horizontal vibrations of the payload. Therefore, this improved the controllability of the crane significantly when compared with these cranes with fixed suspension points.

Observability and controllability are guaranteed using two measurements and three control inputs. The states in addition to the disturbances acting on the payload and the whole ship, which were the force and sea waves motion in the x-direction respectively, are reconstructed by a PI-Observer. Three controllers are run in parallel to suppress the vibrations in the crane and payload; the first and second controller are

the rolling disturbance and sea waves motion in the x-direction compensators; they produce an input command proportional to the measured roll angle and x displacement to prevent the sea motions from transmitting to the payload through the structure of the crane. The third controller is an optimal state feedback controller based on the states reconstructed by the PI-Observer; its duty is to create the necessary damping to dampen out the vibrations due to other effect as nonzero initial conditions or disturbance forces acting on the payload, it is also responsible to suppress the vibrations caused by operator commands (hoisting and lowering the payload).

A variable gain observer and a variable-gain controller are designed to control the crane which represented by a multi-model problem; the numerical values of the gains are updated in real time according to (a) the current operating region, which is determined by the region finder, and (b) the location of the current operating point inside the current region. Each operating region has four corners, and each corner has its own observer and controller gain set. The actual controller and observer gains at any point inside the region are calculated using 2D interpolation polynomial; this ensures a smooth operation of the controller and preserves the stability and performance robustness as demonstrated using the root locus method. In addition, transition of the controller between different operating regions takes place gradually and in a smooth manner because any two successive regions have a common edge of two common nodes. This guaranteed that no step change in the gains occurred and therefore chattering in the response is avoided. Simulation results showed that the expressed control strategy has a significant effect in suppressing the vibrations in the crane for different values of the payload mass.

5.2 Recommendations

For future works and further studies, we recommend the following:

- Include the dynamics of the actuators in the model.
- Extend the mathematical model to include the out of plane motions.
- Consider the boom to be elastic.
- Include the nonlinear terms in the model and use nonlinear control.
- Alternatively, use the PI-Observer to estimate the nonlinearities and compensate their effects.

5.3 References

[1] Al-Sweiti, Y., 2006 "Modeling and Control of an Elastic Ship Mounted Crane Using Variable-Gain Model-Based Controller," Dr.-Ing thesis, Engineering Faculty of Duisburg-Essen, Germany.

[2] Abdel-Rahman, E. and Nayfeh, A., "Feasibility of two dimensional control for ship-mounted cranes," DETC 2001 Proceedings of the ASME Design Engineering Technical Conferences, Pittsburgh, Pennsylvania, DETC 2001/VIB-21454.

[3] Charles L. Phillips, Royce D. Harbror, 2000, "Feedback Control Systems," 4nd ed. Prentice-Hall International, New Jersey, USA.

[4] Dadone, P. and Van Landingham, H. F., 1999, "The use of Fuzzy logic for controlling Coulomb friction in crane swing alleviation," Intelligent Engineering Systems through Artificial Neural Networks 9, 751-756.

[5] Daniel J. Inman. 1989, "Vibration with Control, Measurement, and Stability," Prentice-Hall International, Mexico, pp. 141-182.

[6] Henry, R., Masoud Z., Nayfeh, A., and Mook, D., 2001, "Cargo pendulation reduction on ship-mounted cranes via boom-luff angle actuation," Journal of Vibration and Control 7, 1253-1264.

[7] Holman, J. P., 2001, "Experimental Methods for Engineers," 7th ed., McGraw-Hill, USA.

[8] Jacob Fraden, 2004, "Handbook of Modern sensors, Physics, Design, and Applications," 3rd ed., Springer, New York, USA.

[9] Kimiaghalam, B., Homaifar, A., and Bikdash, M., 1999, "Pendulation suppression of a shipboard crane using fuzzy controller," Proceedings of the American Control Conference, San Diego, CA, Vol. 1, pp. 586-590.

[10] Kimiaghalam, B., Homaifar, A., and Bikdash, M., 2000, "Feedback and Feedforward Control Law for a Ship Crane with Maryland Rigging System," Proceedings of the American Control Conference, Chicago, IL, Vol. 2, pp. 1047-1051.

[11] Gene F. Franklin, J. David Powell, Abbas Emami-Naeini, 2002, "Feedback Control of Dynamic Systems," 4th ed. Prentice Hall, New Jersey.

[12] Krajcin, I., Söffker, D., 2005, "Diagnosis and Control of 3D Elastic Mechanical Structures". In Precedings 12th international Symposium, Smart Structures and Materials: Smart Structures and Integrated Systems, San Diego, USA, 13 pages.

[13] Krajcin, I., Söffker, D., 2005, "Advanced Model-Based Disturbance Rejection Control Using Proportional-Integral-Observer," DETC 2005 ASME 20th Biennial Conference on Mechanical Vibration and Noise (VIB), Long Beach, California, DETC 2005-84997.

[14] Lunze, 2002 "Regelungstechnik2, Mehrgrößensysteme, Digital Reglung" Springer Verlag, Berlin.

[15] Masoud Z., Nayfeh, A., and Mook, D., 2004, "Cargo pendulation reduction of ship-mounted cranes," Nonlinear Dynamics 35, 299-311.

[16] Meirovitch, L. 1986, "Elements of Vibration Analysis," 2nd ed. McGraw-Hill Book Company, New York, Chap. 8, pp. 300-346.

[17] Müller, P. C., Lückel, J., 1997, "Zur Theorie der Störgrößenaufschaltung in linearen Mehrgrößenregelsystemen". Regelungstechnik 25, pp. 54-59.

[18] Müller, P. C., 1998, "Control of nonlinear systems by applying disturbance rejection control techniques". In Proceedings IEE Int. Conference CONTROL 88, Institution of Electrical Engineers, London, pp. 734-737.

[19] Norvelle, F. Don. 2000, "Electrohydraulic Control Systems," Prentice Hall, New Jersey.

[20] Katsuhiko Ogata. 2002, "Modern Control Engineering," 4th ed. Prentice Hall, New Jersey.

[21] Shahrokh Yadegari, 2003, "Chaotic Signal Synthesis with Real Time Control: Solving Differential Equations in PD, MAX/MSP, and JMAX," Proceedings of the 6th Int. Conference on Digital Audio Effects (DAFx-03), London, UK.

[22] Söffker, D., Bajkowski, J. and Müller, P.C., 1993, "Detection of Cracks in Turbo Rotors – a New Observer Based Method". ASME Journal of Dynamic Systems, Measurements and Control 3, pp. 518-524.

[23] Söffker, D., Yu, T. J., Müller, P. C., 1995, "State Estimation of Dynamical Systems with Nonlinearities by using Proportional-Integral Observer". International Journal of System Science, Vol. 26 (9), pp. 1571-1582.